

Role of Diamagnetic Ions on the Mechanism of Magnetization Relaxation in “Butterfly” $\{\text{Co}^{\text{III}}_2\text{Ln}^{\text{III}}_2\}$ (Ln =Dy, Tb and Ho) complexes

Kuduva R. Vignesh¹, Stuart K. Langley², Keith S. Murray^{3*} and Gopalan Rajaraman^{4*}

1) *IITB-Monash Research Academy, IIT Bombay, Mumbai, India.*

2) *School of Science and the Environment, Division of Chemistry, Manchester Metropolitan University, Manchester, UK*

3) *School of Chemistry, Monash University, Victoria 3800, Australia.*

4) *Department of Chemistry, IIT Bombay, Mumbai-400076, India.*

Email:keith.murray@monash.edu and rajaraman@chem.iitb.ac.in

Abstract

The synthesis, magnetic and theoretical studies of three isostructural heterometallic $[\text{Co}^{\text{III}}_2\text{Ln}^{\text{III}}_2(\mu_3\text{-OH})_2(ortho\text{-tol})_4(\text{mdea})_2(\text{NO}_3)_2]$ {Ln = Dy (**1**), Tb (**2**), and Ho (**3**)} “butterfly” complexes are reported [*ortho*-tol = *ortho*-toluate, (mdea)²⁻ = doubly deprotonated N-methyldiethanolamine]. The Co^{III} ions are diamagnetic in these complexes. Dc magnetic susceptibility measurements reveal antiferromagnetic exchange coupling between the two Ln^{III} ions for all three complexes. Ac magnetic susceptibility measurements reveal single-molecule magnet (SMM) behavior for complex **1**, in the absence of an external magnetic field, with an anisotropy barrier U_{eff} of 81.2 cm⁻¹, while complexes **2** and **3** exhibit field induced SMM behavior, with a U_{eff} of 34.2 cm⁻¹ for **2**. The barrier height for **3** could not be quantified as no out-of-phase maxima are observed in the temperature range measured. To understand the experimental observations, we performed DFT and *ab initio* CASSCF+RASSI-SO calculations, to probe the single ion properties, the nature and magnitude of the Ln^{III}-Ln^{III} magnetic coupling and develop an understanding the role the diamagnetic Co^{III} ion plays in the magnetization relaxation. The calculations were able to rationalize the experimental relaxation data for all complexes and strongly suggests that the Co^{III} ion is integral to the observation of SMM behavior in these systems. Thus, we explored further the effect that the diamagnetic Co^{III} ions have on the magnetization blocking of **1**. We did this by modeling a dinuclear {Dy^{III}₂} complex (**1a**), with the removal of the diamagnetic ions, and three complexes of type - {K^I₂Dy^{III}₂} (**1b**), {Zn^{II}₂Dy^{III}₂} (**1c**) and {Ti^{IV}₂Dy^{III}₂} (**1d**) each containing a different diamagnetic ion. We found that the presence of the diamagnetic ions results in larger negative charges on the bridging hydroxides (**1b** > **1c** > **1** > **1d**), compared to **1a** (no diamagnetic ion), which reduces quantum tunneling of magnetization effects allowing for more desirable SMM characteristics. The results also indicate that the monocationic (K^I) and dicationic (Zn^{II}) diamagnetic ions have a larger influence compared to the tricationic (Co^{III}) and tetracationic (Ti^{IV}) diamagnetic ions in magnetization blocking and the magnitude of the energy barriers. Here we propose a synthetic strategy to enhance the energy barrier in lanthanide based SMMs by incorporating s- and d-block diamagnetic ions. The presented strategy is likely to have implications beyond the single-molecule magnets studied here.

Introduction

Lanthanide ions have begun to overshadow d-block transition metals in the development of new molecular magnetic materials, such as single molecule magnets (SMMs).¹ Primarily, the trivalent ions of dysprosium and terbium have been extensively used in the syntheses of new SMMs² because of the strong anisotropy provided by these ions.³ SMM behavior has generated great interest due to the physical properties linked with magnetic hysteresis and quantum tunneling of magnetization (QTM), with potential applications in high density information storage devices,⁴ as Qubits⁵ and ‘Spintronic’ devices.^{5a, 6} The great shift towards lanthanide based SMMs is a result of the observation of extremely large anisotropy barriers,⁷ the magnitudes of which are significantly larger than what has previously been observed for polynuclear 3d clusters.^{6, 8} The anisotropy barrier (U_{eff}) is the energy required to “flip” the orientation of the magnetic moment and return to thermal equilibrium in the ground magnetic micro-states. With such large energy barriers, one would expect to store digital information at temperatures much greater than those currently possible (blocking temperatures of 14 K and 30 K^{9,10}), however this has not materialized due to fast QTM which shortcuts the barrier, resulting in “fast” magnetization reversal. Most lanthanide-based SMMs reported in the literature use Dy^{III} and Tb^{III} because these ions have a large magnetic anisotropy and a lower tendency to exhibit QTM, when compared to other lanthanide ions. To limit QTM further, strong magnetic exchange interactions between polynuclear 4f complexes are favorable and/or the synthesis of 4f single ion sites which display an Ising type magnetic anisotropy, with a minimal transverse component. A representative example of the former, a {Tb₂} complex, displays a U_{eff} value of 226 cm⁻¹, and magnetic hysteresis up to temperatures as high as 14 K,^{9a} while an example of the latter is the report of a pseudo D_{5h} symmetry Dy^{III} complex exhibiting very large magnetic blocking temperatures and negligible transverse terms both in the ground and the first excited states.¹⁰

Recently, heterometallic 3d/4f complexes have been actively studied as an alternate to pure 4f coordination complexes. This area of active research has arisen from recent experimental data that indicate two separate synthetic strategies can be considered. The first approach uses paramagnetic 3d transition metal ions, taking advantage of the combination of the large spin of 3d ions with the spin/anisotropy of the 4f ions.¹¹ More importantly the 3d ions offer the potential to provide stronger magnetic exchange interactions than is possible for pure polynuclear 4f complexes. Such 3d-4f

magnetic exchange interactions have shown to significantly reduce QTM and using 3d ions such as Cr^{III},¹² Fe^{III},¹³ Mn^{III},¹⁴ and Ni^{II},¹⁵ have provided heterometallic 3d-4f SMMs with long relaxation times (> 100 s) up to 4.7 K.^{12a} The second approach utilizes diamagnetic ions in conjunction with Ln^{III} ions. It has been shown that these cations influence the electron density distribution of surrounding coordinating ligands, thus affecting the electronic structure and the single ion magnet properties of the Ln^{III} ion. Systems such as {ZnDy}¹⁶ have provided clear evidence that positively charged diamagnetic ions can help stabilize an Ising type anisotropy for the 4f ion. This strategy has successfully been employed towards the isolation of several Dy^{III} SMMs with attractive barrier heights.¹⁶

Based on the diamagnetic ion approach, one can assume that the Co^{III} ion with a low spin d⁶ electron configuration is therefore an ideal candidate to stabilize heterometallic 3d-4f complexes, containing a high charge diamagnetic ion. Some of us have already reported a family of tetrานuclear {Co^{III}₂Ln^{III}₂} SMMs, where the SMM behavior is influenced by the ligand environment surrounding the Dy^{III} ion. The energy barriers in these complexes were found to range from 14 to 170 K depending on the ligands utilized in the synthesis of the complex.¹⁷ Previous studies on these systems focused heavily on the effect of the ligand, however, no studies have been made to probe the influence/importance of the diamagnetic ion on these SMMs, and in particular how the relaxation can be affected by different diamagnetic ions. In this report we have synthesized a new family of heterometallic {Co^{III}₂Ln^{III}₂} (Ln = Tb, Dy, Ho) complexes using the ligands N-methyldiethanolamine (mdeaH₂) and *ortho*-toluic acid (*ortho*-tolH). The complexes are of general formula - [Co^{III}₂Ln^{III}₂(μ₃-OH)₂(*ortho*-tol)₄(mdea)₂(NO₃)₂] {Ln = Dy(**1**), Tb (**2**), and Ho (**3**)} each containing the diamagnetic Co^{III} ion. We report the synthesis, magnetic properties and provide an *ab initio* and density functional theory (DFT) theoretical description of the three complexes and explore the effect the diamagnetic Co^{III} ion has on the energy barrier to magnetic reversal.

Experimental Section

General Information

All reactions were carried out under aerobic conditions. Chemicals and solvents were obtained from commercial sources and used without further purification.

*Synthesis of [Co^{III}₂Dy^{III}₂(μ₃-OH)₂(*ortho*-tol)₄(mdea)₂(NO₃)₂] (**1**).*

$\text{Co}(\text{NO}_3)_2 \cdot 6\text{H}_2\text{O}$ (0.29 g, 1 mmol) and $\text{Dy}(\text{NO}_3)_3 \cdot 6\text{H}_2\text{O}$ (0.22 g, 0.5 mmol) were dissolved in MeCN (20 mL), followed by the addition of N-methyldiethanolamine (0.1 mL, 1 mmol), *ortho*-toluic acid (0.14 g, 1.0 mmol) and triethylamine (0.55 mL, 4.0 mmol), which resulted in a dark green solution. This solution was stirred for four hours, after which the solvent was removed, resulting in a green oil. The oil was re-dissolved in MeOH/iPrOH (1:1) and layered with diethyl ether (Et_2O). Within 8–10 days, green crystals of **1** had appeared, in approximate yield of 65 % (crystalline product). Microanalysis for $\text{Co}_2\text{Dy}_2\text{C}_{42}\text{H}_{52}\text{N}_4\text{O}_{20}$: Expected (found); C 36.67 (36.86), H 3.81 (3.86), N 4.07 (4.32).

Synthesis of $[\text{Co}^{III}_2\text{Tb}^{III}_2(\mu_3\text{-OH})_2(\text{ortho-tol})_4(\text{mdea})_2(\text{NO}_3)_2]$ (2). The synthesis for **1** was followed but $\text{Tb}(\text{NO}_3)_3 \cdot 6\text{H}_2\text{O}$ (0.17 g, 0.5 mmol) was used in place of $\text{Dy}(\text{NO}_3)_3 \cdot 6\text{H}_2\text{O}$. Dark green crystals of **2** appeared within 10–15 days, in approximate yield of 47 % (crystalline product). Microanalysis for $\text{Co}_2\text{Tb}_2\text{C}_{42}\text{H}_{52}\text{N}_4\text{O}_{20}$: Expected (found); C 36.86 (36.34), H 3.83 (3.67), N 4.09 (4.23).

Synthesis of $[\text{Co}^{III}_2\text{Ho}^{III}_2(\mu_3\text{-OH})_2(\text{ortho-tol})_4(\text{mdea})_2(\text{NO}_3)_2]$ (3). The synthesis for **1** was followed but $\text{Ho}(\text{NO}_3)_3 \cdot 6\text{H}_2\text{O}$ (0.22 g, 0.5 mmol) was used in place of $\text{Dy}(\text{NO}_3)_3 \cdot 6\text{H}_2\text{O}$. Dark green crystals of **3** appeared within 10–12 days, an approximate yield of 52 % (crystalline product). Microanalysis for $\text{Co}_2\text{Ho}_2\text{C}_{42}\text{H}_{52}\text{N}_4\text{O}_{20}$: Expected (found); C 36.53 (36.71), H 3.80 (3.93), N 4.06 (4.11).

X-ray crystallography

Single crystal X-ray diffraction measurements for **1** and **2** were performed at 100(2) K at the Australian synchrotron MX1 beam-line.¹⁸ Data collection and integration were performed in Blu-Ice¹⁹ and XDS²⁰ software programs. Compounds **1** and **2** were solved by direct methods (SHELXS-97),²¹ and refined (SHELXL-97)²² by full least-matrix least-squares on all F2 data.²³ Crystallographic data and refinement parameters for **1** and **2** are summarized in Table 1. CCDC numbers 1510217 (**1**) and 1510218 (**2**). These data can be obtained free of charge from the Cambridge Crystallographic Data Centre via www.ccdc.cam.ac.uk/data_request/cif. Powder X-ray diffraction measurements were performed for complex **3** and were measured on a Bruker X8 Focus powder diffractometer using the Cu K α wavelength (1.5418 Å). The samples were mounted

on a zero-background silicon single-crystal stage. Scans were performed at room temperature in the 2θ range $5 - 55^\circ$ and compared with predicted patterns based on low-temperature single-crystal data.

Magnetic measurements

Magnetic susceptibility measurements were carried out on a Quantum Design SQUID magnetometer MPMS-XL 7, which operated between 1.8 and 300 K for dc-applied fields that range from 0 – 5 T. Microcrystalline samples were dispersed in Vaseline in order to avoid torquing of the crystallites. The sample mulls were contained in a calibrated gelatine capsule held at the centre of a drinking straw that was fixed at the end of the sample rod. Alternating current (ac) susceptibilities were carried out under an oscillating ac field of 3.5 Oe with frequencies ranging from 0.1 to 1500 Hz.

Computational details

Ab initio calculations:

Using MOLCAS 7.8,²⁴ *ab initio* calculations were performed on the trivalent lanthanide ions; Dy, Tb and Ho, using the single crystal structural data. In complexes **1–3**, the anisotropy of a single Ln^{III} ion was calculated on the basis of the X-ray determined geometry and by replacement of the neighboring Ln^{III} ion with a diamagnetic La^{III} ion. Relativistic effects are taken into account on the basis of the Douglas–Kroll Hamiltonian.²⁵ The spin-free Eigen states are achieved by the Complete Active Space Self-Consistent Field (CASSCF) method.²⁶ We have employed the [ANO-RCC... 8s7p5d3f2g1h.] basis set²⁷ for Dy, Tb and Ho atoms, the [ANO-RCC...3s2p.] basis set for C atoms, the [ANO-RCC...2s.] basis set for H atoms, the [ANO-RCC...3s2p1d.] basis set for N atoms, the [ANO-RCC...5s4p2d.] basis set for Co, K, Zn and Ti atoms and the [ANO-RCC...3s2p1d.] basis set for O atoms. The CASSCF calculations that were performed included nine electrons across seven 4f orbitals of the Dy³⁺ ion, eight electrons across seven 4f orbitals of the Tb³⁺ ion, and ten electrons across seven 4f orbitals of the Ho³⁺ ion in **1**, **2** and **3**, respectively. With this active space, 21 roots in the Configuration Interaction (CI) procedure were computed for complex **1**. We also considered seven septet excited states, one hundred and forty quintet excited states and one hundred and ninety-five triplet excited states for complex **2**, and thirty-five quintet

excited states, two hundred and ten triplet excited states and one hundred and ninety-five singlet excited states for complex **3** in the calculations to compute the anisotropy.

After computing these excited states, we mixed all roots using RASSI-SO²⁸; spin-orbit coupling is considered within the space of the calculated spin-free eigenstates for **2** and **3**. Moreover, these computed SO states have been considered into the SINGLE_ANISO²⁹ program to compute the *g*-tensors. The anisotropic *g*-tensors for the Dy^{III} ion, the Tb^{III} ion and the Ho^{III} ion have been computed with eight, seven and eleven low-lying doublets. Cholesky decomposition for two electron integrals is employed throughout our calculations. Crystal-field parameters have been extracted using the SINGLE_ANISO code, as implemented in MOLCAS 7.8. The exchange interactions have been computed between the Ln^{III} ions within each complex by fitting with the experimental data using the Lines model and employing the POLY_ANISO module.³⁰

In addition to studying complexes **1 – 3**, we have modeled a dinuclear {Dy^{III}₂} unit using the crystal structure of **1** to explore the effect the diamagnetic Co^{III} ions have on magnetization blocking of **1**. The structure of the model complex is reported as **1a**. Furthermore, we have modeled three further complexes; {K^I₂Dy^{III}₂} (**1b**), {Zn^{II}₂Dy^{III}₂} (**1c**) and {Ti^{IV}₂Dy^{III}₂} (**1d**), using the X-ray structure of **1** by replacing the Co^{III} ions with K^I, Zn^{II} and Ti^{IV} ions, respectively, to explore the effect that other cationic diamagnetic ions of varying charge have on the magnetic properties and how they compare with the tricationic diamagnetic ion (Co^{III}) in magnetization blocking.

Density Functional Theory calculations

The exchange interaction between Ln^{III} ions has been validated using the density functional theory (DFT) method by replacing the Dy^{III} ions with Gd^{III} (**1e**) ions and keeping the positions of the other atoms the same as determined by the X-ray structure of **1**. The DFT method has also been utilized to predict the Mulliken spin charges of the modeled structures {Gd^{III}₂} (**1f**) and {Zn^{II}₂Gd^{III}₂} (**1g**). The DFT calculations combined with the Broken Symmetry (BS) approach³¹ has been employed to compute the *J* value of these complexes. The BS method has a proven record of yielding good numerical estimates of *J* constants for a variety of complexes³² such as dinuclear³³ and polynuclear complexes.^{14c, 32a, 34} The DFT calculations were performed using the B3LYP functional³⁵ with the Gaussian 09 suite of programs.³⁶ We have employed the double-zeta quality basis set that employs the Cundari-Stevens (CS) relativistic effective core potential on the

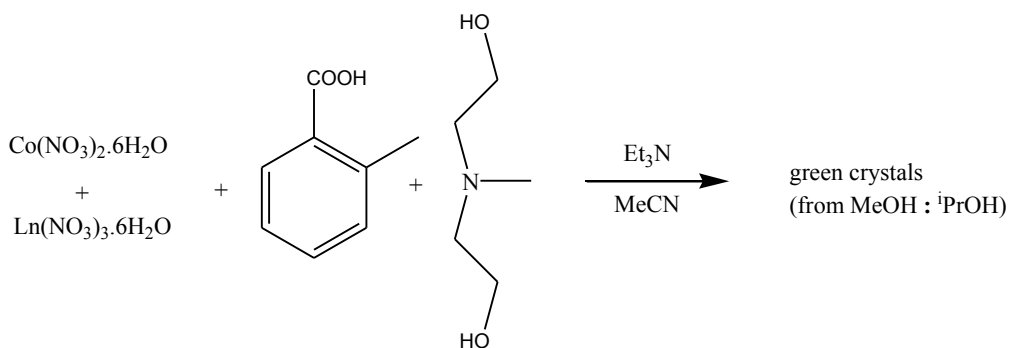
Gdatom³⁷, and Ahlrich's³⁸ triple- ζ -quality basis set for the rest of the atoms. The following Hamiltonian is used to estimate the exchange interaction (J) in **1c**.

The computed exchange coupling constants for the Gd^{III}-Gd^{III} pair was rescaled to the spin of the Dy^{III} ion by multiplying them by spin of Dy^{III} ($S = 5/2$) and dividing by spin of Gd^{III} ($S = 7/2$).^{12b} Similarly, the Gd^{III}-Gd^{III} pair was rescaled for the Tb ion ($S = 3$) and the Ho ion ($S = 2$). The resultant J values are in good agreement with the fitted values.

RESULTS AND DISCUSSION

Synthesis and crystal structures

The reaction of $\text{Co}(\text{NO}_3)_2 \cdot 6\text{H}_2\text{O}$ and $\text{Ln}(\text{NO}_3)_3 \cdot 6\text{H}_2\text{O}$ ($\text{Ln} = \text{Dy, Tb, and Ho}$) with mdea H_2 and *ortho*-toluic acid in acetonitrile, followed by the removal of the solvent and re-dissolution in a MeOH/*i*PrOH (1:1), yielded green crystals from solution when layered with diethyl ether. Analysis of the single crystal x-ray data revealed a family of tetranuclear butterfly complexes of general formula $[\text{Co}^{\text{III}}_2\text{Ln}^{\text{III}}_2(\mu_3\text{-OH})_2(\text{ortho-tol})_4(\text{mdea})_2(\text{NO}_3)_2]$ ($\text{Ln} = \text{Dy(1); Tb(2), and Ho(3)}$). This family of complexes is a variation of previously reported $\{\text{Co}^{\text{III}}_2\text{Ln}^{\text{III}}_2\}$ butterfly complexes.^{17, 39} Two $[\mu_3\text{-OH}]^-$ bridging ligands are now present in place of $[\mu_3\text{-OMe}]^-$, a consequence of the choice of solvent used for crystallization and *ortho*-toluic acid is used for the first time as the choice of carboxylic acid.



Scheme 1. Reaction scheme used to isolate tetranuclear compound **1 – 3**.

Compounds **1** and **2** are isostructural (See Table S1 for crystallographic details of **1** and **2**), however, suitable single crystals for the X-ray diffraction could not be obtained for **3** and therefore the isostructural nature and purity of **3** was determined by powder X-ray diffraction

(Figure S1). A description of the Dy^{III} analogue **1** will be given here and is representative of **1 – 3**. Complex **1** (Figure 1) is a heterometallic tetranuclear complex that crystallises in the triclinic space group, *P-1*; the asymmetric unit contains one-half of the complex, which lies upon an inversion centre. The metallic core consists of two Co^{III} and two Dy^{III} ions, displaying a planar “butterfly” (or diamond) motif. The Dy^{III} ions occupy the body positions, and the Co^{III} ions the outer wing-tips (Figure 1). The core is stabilised by two μ_3 -hydroxide ligands, both bridging to two Dy^{III} ions and one Co^{III} ion. Around the periphery of the cluster, there are four *ortho*-toluate ligands, bridging a Co^{III} to a Dy^{III} ion. There are also two doubly deprotonated (mdea)²⁻ ligands, with the N-atom coordinating to an outer Co^{III} ion, with the two O-atoms bridging from the Co^{III} to the body Dy^{III} ions. Both the Dy^{III} ions are chelated by a (NO₃)⁻ ligand through two O-atoms. The two Co^{III} ions are six coordinate with octahedral geometries, and the two Dy^{III} ions are eight coordinate with distorted square antiprismatic geometries as identified using the SHAPE program (See theoretical section, *vide infra*).⁴⁰ The packing diagrams of **1** and **2** reveal offset aromatic π - π intercluster interactions (highlighted by the dashed lines in the Figure S2).

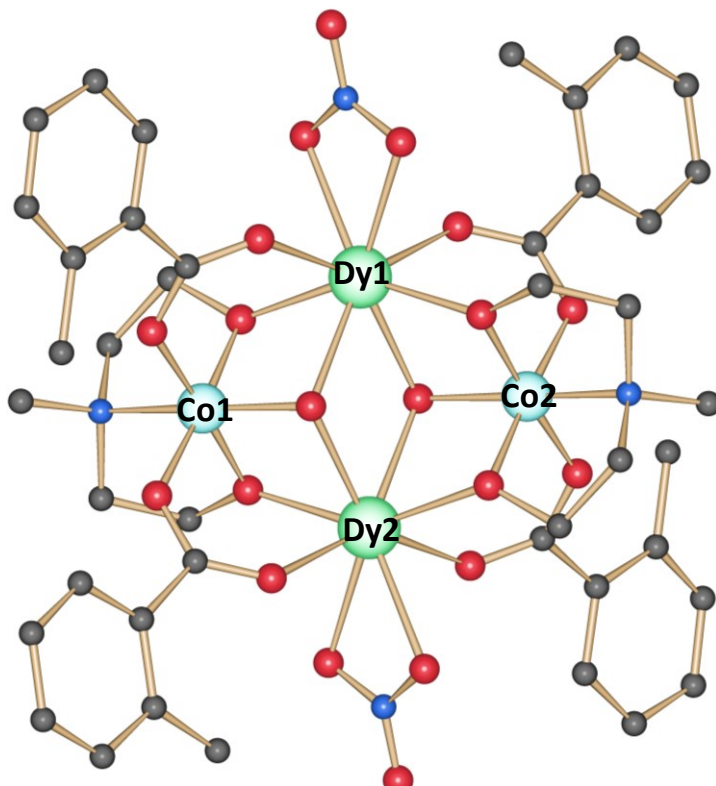


Figure 1. The molecular structure of complex **1**. The solvent and H atoms are omitted for clarity. Colour scheme:Co^{III}, skyblue; Dy^{III}, green; O, red; N, blue; C, light grey. Complexes

2 and **3** are isostructural to **1**, with the Tb^{III} and Ho^{III} ions replacing the Dy^{III} sites.

Magnetic properties

Direct current magnetic susceptibility measurements

The variation of the direct current (dc) magnetic susceptibility product $\chi_M T$ versus temperature for complexes **1** – **3** is shown in Figure 2. The room temperature $\chi_M T$ values of 28.14, 23.68 and 28.22 cm³ K mol⁻¹ for **1**, **2** and **3** are in good agreement with the value expected for two Dy^{III} ($S = 5/2$, $L = 5$, $^6H_{15/2}$, $g = 4/3$, $C = 14.17 \text{ cm}^3 \text{ K mol}^{-1}$), two Tb^{III} ($S = 3$, $L = 3$, 7F_6 , $g = 3/2$, $C = 11.82 \text{ cm}^3 \text{ K mol}^{-1}$) and two Ho^{III} ($S = 2$, $L = 6$, 5I_8 , $g = 5/4$, $C = 14.075 \text{ cm}^3 \text{ K mol}^{-1}$) ions, of 28.34 cm³ K mol⁻¹, 23.64 cm³ K mol⁻¹ and 28.15 cm³ K mol⁻¹, respectively. The decrease of the $\chi_M T$ product (at $H_{dc} = 1$ T) for **1** – **3**, from room temperature to 1.8 K, is indicative of the presence of thermal depopulation of the Ln^{III} m_J levels, combined perhaps with weak antiferromagnetic interactions between the Ln^{III} ions (see later for the analysis of the Ln^{III}–Ln^{III} magnetic exchange interaction). The isothermal magnetization M vs H plots reveal similar profiles (Figure S3), for **1** – **3**, with a rapid increase in magnetization below 2 T, before following a more gradual linear-like increase, without saturating, thus signifying a significant anisotropy and/or low lying excited states are present.

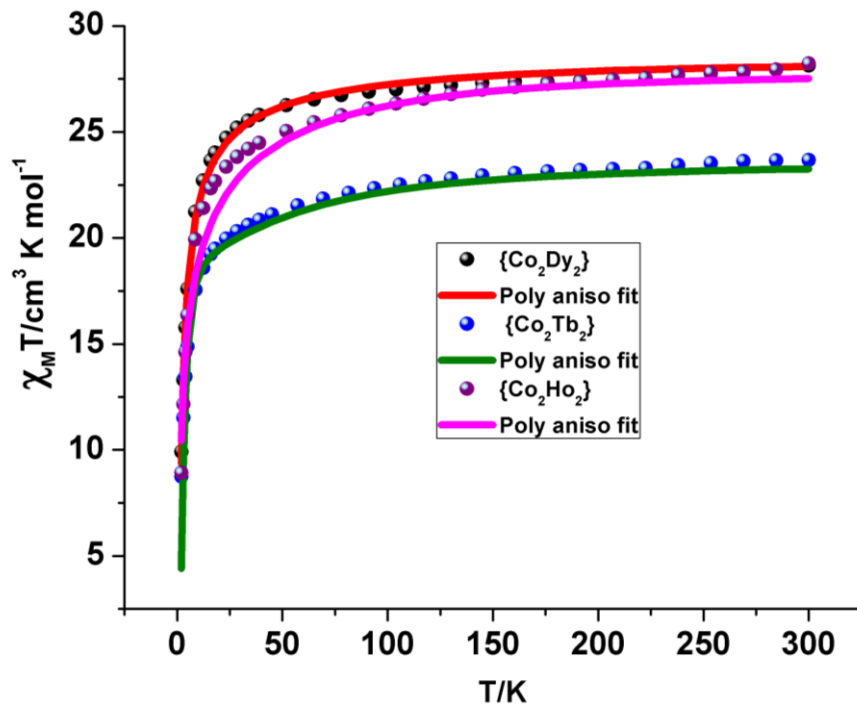


Figure 2. Plots of $\chi_M T$ versus T plots for **1 – 3** (dotted line). The solid lines are fits of the data using the Lines model employing the POLY_ANISO program

Alternating current magnetic susceptibility measurements

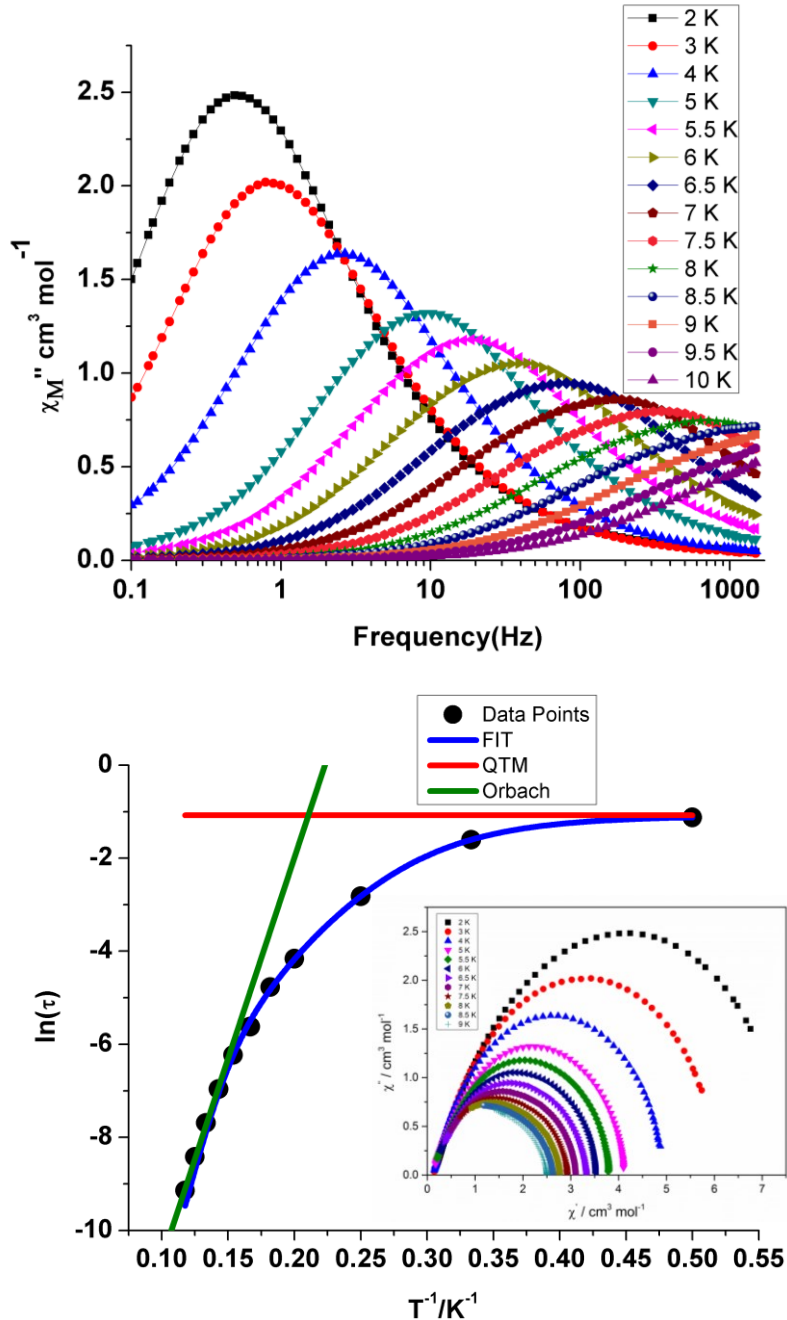


Figure 3. (top) Frequency dependence of χ_M'' for **1** in a zero applied dc field, with an ac magnetic field of 3.5 Oe; (bottom) Magnetization relaxation time (τ), plotted as $\ln(\tau)$ versus T^{-1} for compound **1**. The solid green line corresponds to fitting of the Orbach relaxation process and the solid blue

line represents the fitting to multiple relaxation processes. The horizontal red line represents the QTM relaxation time; (bottom inset) Cole–Cole plots between 2 – 9 K.

Alternating current (ac) magnetic susceptibility experiments were performed to investigate the dynamics of relaxation of the magnetization. Measurements for compound **1** were implemented in an ac magnetic field of 3.5 Oe, oscillating at frequencies ranging from 0.1–1500 Hz and at temperatures between 2 and 17 K. The plot of χ_M'' versus frequency (ν) reveals temperature-dependent out-of-phase (χ_M'') susceptibility signals confirming the presence of slow relaxation of the magnetization for **1**, and SMM behavior (Figure 3, top). Peak maxima are observed for χ_M'' between 2 – 8 K which are found to be temperature-dependent over the entire frequency range. From these data magnetization relaxation times (τ) are extracted. From the frequency-dependent behavior, it was found that the relaxation follows a thermally activated mechanism above 6 K, and the plot of $\ln(\tau)$ vs $1/T$ is shown in Figure 3, bottom. Below 5.5 K, the plot deviates from linearity, indicating that QTM and possibly other relaxation mechanisms are becoming active. It is found at 2 K, the relaxation becomes close to being independent of temperature, indicating a crossover to a pure quantum tunneling mechanism of relaxation. The magnetic relaxation data were treated with the various relaxation processes with the following general equation employed,

$$[1/\tau = 1/\tau_{\text{QTM}} + AT + CT^n + \tau_o^{-1} \exp(U_{\text{eff}}/k_B T)],$$

where the first term corresponds to the relaxation process via a quantum tunneling pathway, the second term models the direct process, the third term corresponds to relaxation via a Raman process, and the fourth term accounts for the Orbach relaxation pathway. Many fits were attempted using a number of variable parameters in the equation. The linear fit (indicated in solid green line) corresponds exclusively to the Orbach relaxation pathway. The best fit for the Arrhenius plot could be obtained considering the Orbach and Raman relaxation process, with the value of the Raman exponent n , closer to 6. The values obtained from the best fit are $n = 6.6$ (T), $C = 0.00013 \text{ s}^{-1} \text{ K}^{-3}$ (T), $U_{\text{eff}} = 116.9$ (2) K (81.2 cm^{-1}) and $\tau_o = 9.8 \times 10^{-9} \text{ s}$ ($R = 0.9997$). This result indicates a large **barrier to thermal relaxation, with a pre-exponential factor of between 10^{-6} and 10^{-11} s, that** is consistent with that expected of an SMM.² A QTM relaxation time, τ_{QTM} , of 0.34 s is estimated.

The Cole–Cole plots of χ_M' versus χ_M'' data reveal semicircular profiles indicating a single relaxation process at temperatures 2 - 9 K (Figure 3, bottom (inset)).

Ac magnetic measurements for the isostructural analogues **2** and **3** reveal an absence of out-of-phase susceptibility peaks in a zero static dc field, but show out-of-phase (χ_M'') susceptibility signals in the presence of applied static dc fields of 5000 Oe and 2000 Oe, respectively (Figure 4 (left) and Figure S4). The absence of SMM behavior in zero magnetic field is attributed to fast QTM. This relaxation pathway can, to some extent, be suppressed upon the application of a static dc magnetic field, which is observed for **2** and **3** allowing for the observation of the thermally activated relaxation mechanism. Analysis of the relaxation data for **2** revealed that the plot of $\ln(\tau)$ vs $1/T$ is linear above 3.1 K, before deviating from linearity below these temperatures - crossing over from a thermally activated process to a quantum tunneling relaxation regime (Figure 4, right). Fitting to the Arrhenius law [$\tau = \tau_0 \exp(U_{\text{eff}}/k_B T)$] afforded values of $U_{\text{eff}} = 49.2$ K (34.2 cm^{-1}) and $\tau_0 = 6.6 \times 10^{-11} \text{ s}$ ($R = 0.9153$).

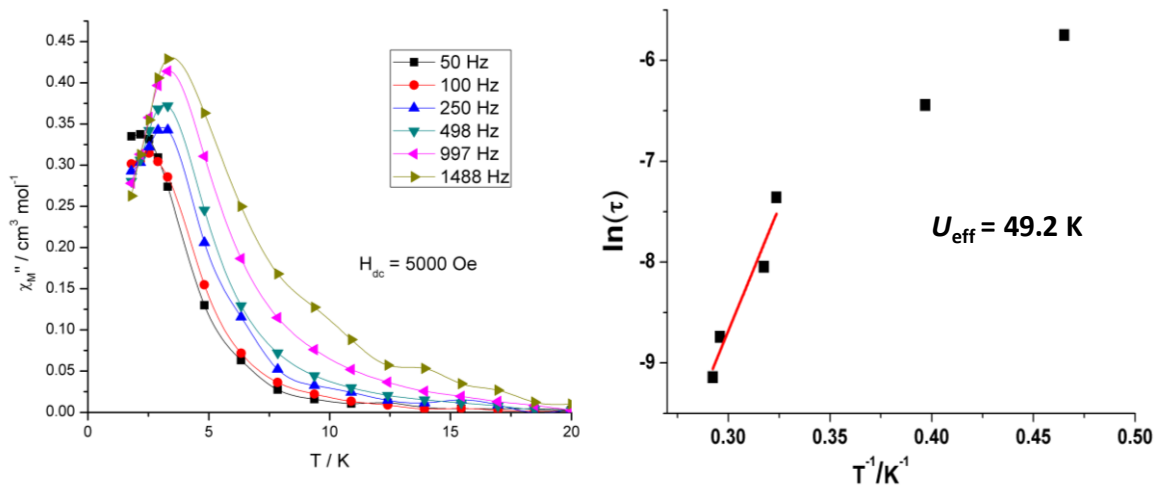


Figure 4. (left) Plot of χ_M'' versus T at the frequencies indicated for **2**, with $H_{dc} = 5000$ Oe; (right) Magnetization relaxation time (τ), plotted as $\ln(\tau)$ versus T^{-1} for compound **2** from the ac data provided on the left.

The anisotropy barrier of **1** ($81.2 \text{ cm}^{-1}/116.9 \text{ K}$) falls within the range of that previously reported for $\{\text{Co}^{\text{III}}_2\text{Dy}^{\text{III}}_2\}$ butterfly complexes (14 – 170 K).¹⁷ The loss of SMM behavior for **2** and **3** in a 0 Oe dc field is a common problem for non-Kramer's ions such as Tb^{III} and Ho^{III} and is a problematic finding as it precludes the use (in most cases) of the extremely large anisotropy both these ions possess.⁴¹ To understand the loss of slow magnetic relaxation, we have performed *ab*

initio calculations to probe the electronic structure of **1 – 3**. Further to this, we have used *ab initio* methods to probe the role the Co^{III} ion plays in the stabilization of the slow magnetic relaxation of **1**. After recently investigating the influence of diamagnetic 3d ions on the SMM properties of heterometallic 3d-4f complexes, we found that the diamagnetic ion has a significant influence on the electronic structure of the Ln^{III} ion(s) and thus on the magnetic relaxation behavior.^{16d} In our previous {Co^{III}₂Ln^{III}₂} work we assumed that the diamagnetic Co^{III} ions did not contribute to the slow magnetic relaxation behavior of the complex.¹⁷ However in the light of recent findings we have hypothetically probed the electronic structure of **1** in the absence of the two Co^{III} ions to see how these ions influence the SMM behavior. Furthermore, we have also investigated what effect replacing the tricationic diamagnetic Co^{III} ion with monocationic K^I, dicationic Zn^{II} and tetracationic Ti^{IV} diamagnetic ions have on the SMM behavior/properties. As noted above, we have labeled these model structures as **1a** (no diamagnetic ion), **1b** (K^I ions), **1c** (Zn^{II} ions) and **1d** (Ti^{IV} ions) (Figure 5).

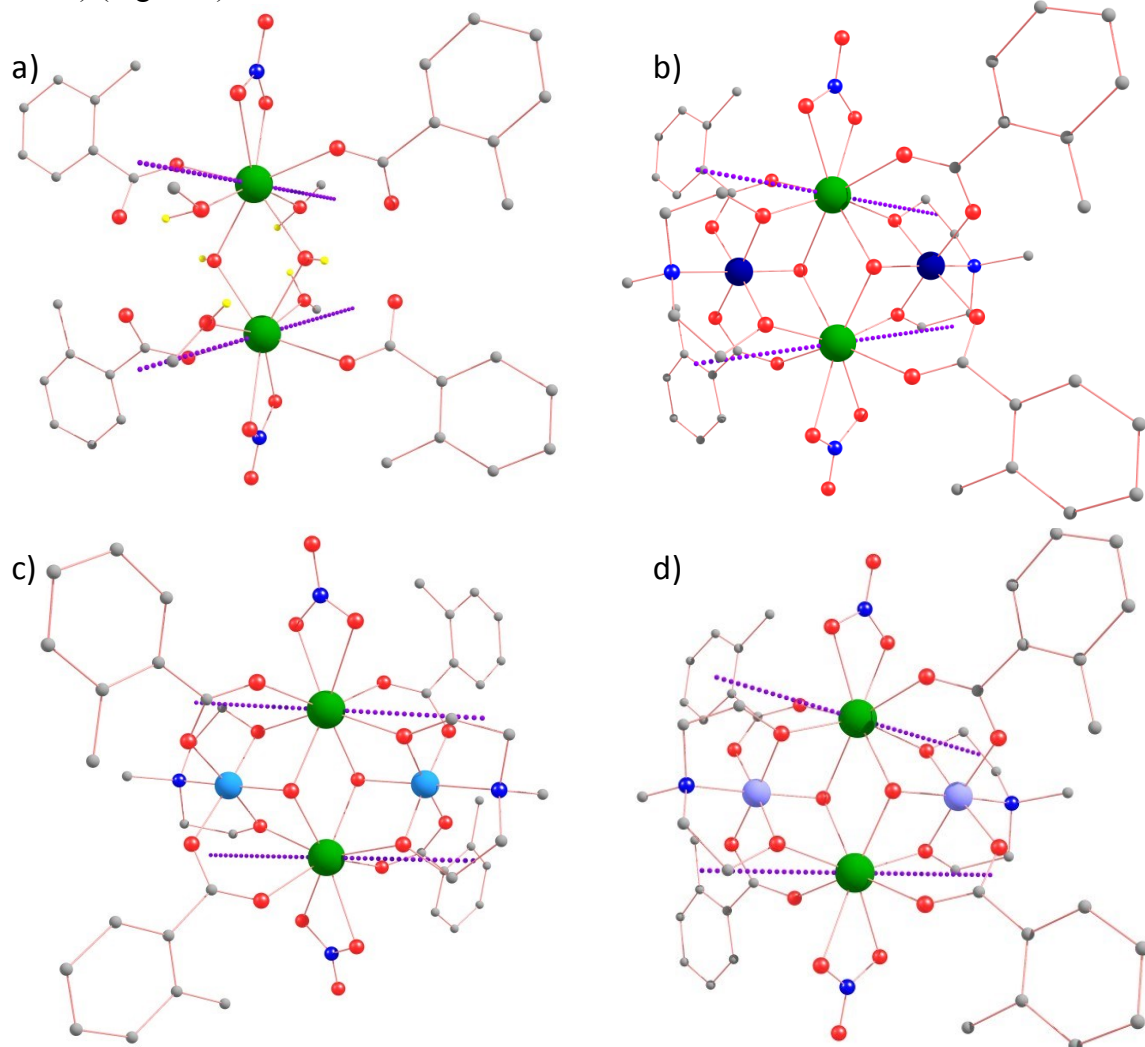


Figure 5. The modelled structure of complex (a) **1a** (b) **1b** (c) **1c** and (d) **1d**. Most of the H atoms are omitted for clarity. Colour scheme: Dy^{III}, green; K^I, Dark blue; Zn^{II}, sky blue; Ti^{IV}, pale violet; O, red; N, blue; C, light grey; H, yellow. The dotted violet lines are the g_{zz} direction of Dy^{III} ions.

Anisotropy calculations

Ab initio calculations on complexes **1** – **3** were performed with the MOLCAS 7.8 program²⁴ of the CASSCF/RASSI-SO/SINGLE_ANISO type. Calculations for **1** and **2** were computed using their X-ray structures, while for complex **3**, the X-ray structure of complex **2** was utilized. In all these calculations the neighboring Ln^{III} ion was computationally substituted by a diamagnetic La^{III} ion. Because the Co^{III} ions are diamagnetic (**1** - **3**) these were not altered in all calculations (see computational details). Initially, a relaxation mechanism based on the single ion anisotropy of the lanthanide ions will be discussed and this will be followed by the analysis of the dinuclear framework, incorporating the weak magnetic exchange coupling between the two Ln^{III} centers. At very low temperatures, the coupled systems are likely to give a realistic picture, however at higher temperatures, where the thermal energies are much greater than the exchange coupling, one can expect the relaxation from individual Ln^{III} ions to be operational.

Table 1. Low-lying energies (cm⁻¹) and g -tensors of the Ln^{III} fragments that originate from the corresponding ground atomic multiplet in **1-3**.

	Dy1	Dy2	Tb1	Tb2	Ho1	Ho2
0.000	0.000	0.000	0.000	0.000	0.000	0.000
77.518	77.944	0.180	0.180	4.496	2.803	
187.362	188.428	138.003	138.003	30.500	21.383	
245.927	247.047	143.825	143.825	47.445	35.528	
273.979	275.357	224.498	224.498	66.331	81.147	
350.793	351.836	275.607	275.607	97.271	112.692	
414.201	415.025	301.178	301.178	109.880	128.906	
675.248	675.816	430.456	430.456	155.589	181.827	
		432.902	432.902	161.296	189.002	
		586.366	586.366	194.535	209.606	
		586.853	586.853	210.938	220.977	
	Ground Kramers Doublet		Ground Ising doublets		Ground Ising doublets	
g_x	0.0005	0.0004	0.0000	0.0000	0.0000	0.0000

g_y	0.0043	0.0043	0.0000	0.0000	0.0000	0.0000
g_z	19.9331	19.9282	17.2555	17.2515	16.1007	16.6344

Ac magnetic susceptibility measurement reveal SMM behavior for complex **1** and the possibility of SMM behavior for **2** and **3**. As slow magnetic relaxation behavior often originates from the anisotropy of the individual Ln^{III} ions, we have quantitatively explored the anisotropy of both Ln^{III} centers in **1–3** using *ab initio* methods. The coordination environment and geometry of each individual Ln^{III} ion was probed using the SHAPE program,⁴⁰ which revealed that the Ln^{III} ions are in a similar environment for each complex. The coordination geometry is best described by a square antiprism. A minor deviation of 2.0 for the Dy^{III} ions in **1** and 2.1 for Tb^{III} ions in **2** are observed with respect to the square antiprism. The calculated electronic and magnetic properties of both Ln^{III} ions suggest that the local g -tensors in the ground Kramer's doublet (KDs) for **1** and ground Ising doublets (**2** and **3**) are strongly axial revealing a large g_z value (see Tables 1 and S3), suggesting that the single ion anisotropy can lead to the slow magnetic relaxation in **1 – 3**. The orientations of the main anisotropy axes in the ground doublets for **1 – 3** are shown in Figure 6. It is found that the directions of the main anisotropy axes in **1** are parallel to the $\text{Co}\cdots\text{Co}$ vector, lying approximately in the direction of the O-Dy-O bond (methoxy O-atoms of the mdea²⁻ ligands), tilted by 24.1° from the O-Dy-O bond vector. However, in complexes **2** and **3**, the g_{zz} axis are found to deviate significantly from the $\text{Co}\cdots\text{Co}$ vector and lie in the direction of the O_{o-tol}-Tb^{III} and O_{o-tol}-Ho^{III} bonds. For complex **3** the orientation of the anisotropy axis of each individual Ho^{III} ion are found to be different and this is reflected in the computed g anisotropy.

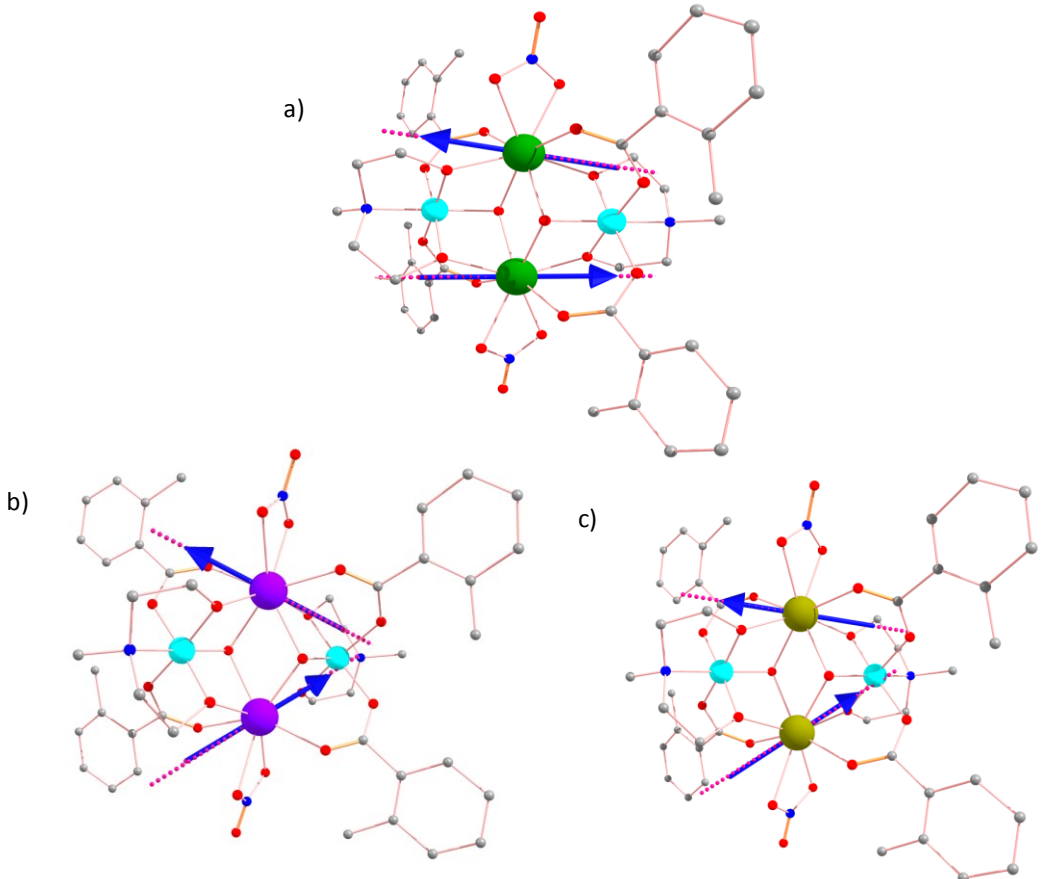


Figure 6. Orientations of the local magnetic moments in the ground doublet of complexes a) **1**; b) **2** and c) **3**. Blue arrows show the antiferromagnetic coupling of the local magnetic moments of the Ln^{III} ions in the ground state (*vide infra*).

The computed energy gap between the ground KDs or the Ising doublets and the excited states are shown in Table 1 and Table S2. The presence of small QTM ($0.8 \times 10^{-3} \mu_{\text{B}}$) at the ground state for both Dy^{III} ions in **1** causes magnetic relaxation to occur via excited KD's. At the first excited state, however, thermally activated-QTM/Orbach processes are operative and thus the magnetization relaxes back to the ground state from the first excited state. The average of the computed energies of the first excited Kramer's doublet for the two Dy^{III} ions in **1** correlate to an energy barrier (U_{eff}) of 77.7 cm^{-1} . This is in good agreement with the experimentally determined barrier (81.2 cm^{-1}), although the experimental value is slightly overestimated and is probably due to the exclusion of intermolecular and hyperfine interactions in the calculation and the possibility of a non-Orbach relaxation mechanism. A qualitative mechanism for the magnetic relaxation for the two Dy^{III} sites in **1** obtained from the *ab initio* calculations is shown in Figure 7. For complexes **2** and **3**, however,

we discover from the calculations that the tunneling gap between the ground state single ion Tb^{III} and Ho^{III} sites are very large $\sim 0.18\text{ cm}^{-1}$ (for **2**) and $2.8 - 4.5\text{ cm}^{-1}$ (for **3**) (see Table 1). This supports the experimental absence of SMM behavior in zero dc field for **2** and **3**. The application of a dc field can lift the degeneracy of the Ising doublets and quench QTM to a certain extent. This is found to be the case from the experiments. As the tunnel splitting parameter in complex **3** ($2.8 - 4.5\text{ cm}^{-1}$) is an order magnitude larger than that estimated for complex **2** (0.18 cm^{-1}), it fits nicely with the experimental observation that complex **2** exhibits maxima in the out-of-phase signal when a moderate dc field is applied, whereas complex **3** does not.

Figure 7. The magnetization blocking barrier for (left) the Dy1 site (right) and the Dy2 site in **1** computed *ab initio*. The thick black line indicates the Kramer's doublets (KDs) as a function of computed magnetic moment. The green/blue arrows show the possible pathway through Orbach/Raman relaxation. The dotted red lines represent the presence of QTM/TA-QTM between the connecting pairs. The numbers provided at each arrow are the mean absolute value for the corresponding matrix element of the transition magnetic moment. The yellow curve indicates the most possible relaxation pathway.

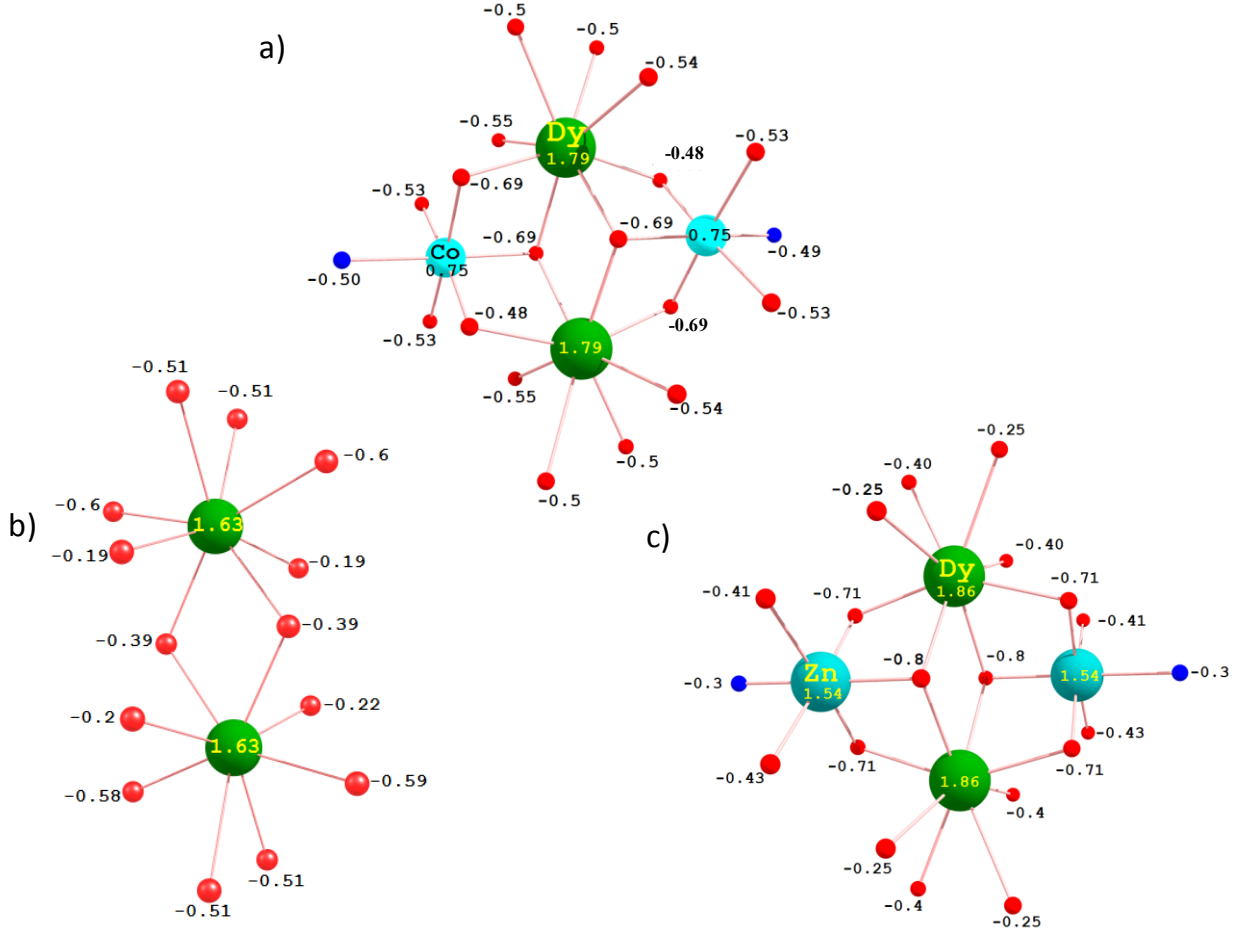


Figure 8. DFT-computed Mulliken charges on the donor atoms of complex a) **1**, b) **1a** and c) **1c**.

The ground state Kramer's doublet of the Dy^{III} ions are estimated to be pure $m_J = \pm 15/2$ ($g_z \sim 20$). The Tb^{III} ion ground doublet is $m_J = \pm 6$ ($g_z \sim 18.0$) and the Ho^{III} ground state resembles that of a $m_J = \pm 7$ state, as the computed anisotropy is close to $g_z \sim 17.5$, but far from the pure $m_J = \pm 8$ state of $g_z \sim 20$. The computed Mulliken charges for complex **1** are shown in Figure 8 a). Among all the coordinated atoms, the largest charges are noticed on the μ_2 and μ_3 -alkoxo oxygen atoms connected to the Co^{III} ion. As the Dy^{III} ion electron density has an oblate shape, the β -electron density will lie perpendicular to the direction of maximum electrostatic repulsion, while the g_{zz} axis lies along the atoms possessing the “largest” charges. This rationalizes the observation of the parallel g_{zz} orientation observed in complex **1**. The “larger” charges found on the alkoxo oxygen atoms, compared to other ligand O-atoms are due to their vicinity of the diamagnetic Co^{III} ion which

polarizes the oxygen atoms. The charge of the ligand donor atoms also influences the crystal field splitting, with the first excited state found 77.5 cm^{-1} higher in energy.

As the electrostatic interactions are the same for the Tb^{III} and Ho^{III} complexes, compared to **1**, one can expect a similar picture. However, Tb^{III} is relatively more oblate than Dy^{III} , while Ho^{III} is less oblate compared to Dy^{III} .^{3a, 42} This means that the electrostatic repulsion of the strongly negative oxygen atoms connected to the Co^{III} ion will have the strongest influence on the electronic structure of the Tb^{III} ions, followed by Dy^{III} and have the weakest influence on the Ho^{III} ions. This is clearly reflected in the ground state-first excited state energy gaps, where the single ion Tb^{III} energy gap is calculated to be 138.0 cm^{-1} , whereas the Dy^{III} energy gap is approximately half of this value at 77.5 cm^{-1} , with the Ho^{III} single ion energy splitting being the smallest at 30 cm^{-1} . Based on this evidence, one can expect SMM behavior with longer relaxation times (at a fixed temperature) to be observed for the Tb^{III} complex, followed by the Dy^{III} complex and the Ho^{III} complex to have the fastest relaxation time if a thermally activated process was favored. However, the magnetic relaxation in lanthanide based complexes is dominated by QTM relaxation pathways and as Tb^{III} and Ho^{III} are non-Kramer's ions, the tunneling, as indicated above, plays a prominent role in quenching the magnetization blockade.

Table 2. Magnetic exchange interactions (cm^{-1}) between magnetic Lanthanide ions in **1–3**.

Magnetic Interactions ($\text{Ln}^{\text{III}}-\text{Ln}^{\text{III}}$)	Calculated	Lines
	$J_{\text{exch}}(\text{DFT})$	J_{exch}
Complex 1	-0.029	-0.05
Complex 2	-0.034	-0.042
Complex 3	-0.023	-0.012

To understand the role of the magnetic exchange interaction between the 4f ions in governing the magnetization relaxation, we have analysed the magnetic exchange using the POLY_ANISO routine.³⁰ The exchange interactions were calculated within the Lines model,⁴³ which describes the exchange coupling between the spin moments of magnetic sites in **1 – 3**. The calculations reproduce the susceptibility and magnetization measurements well; fits of the magnetic data are shown in Figure 2. The exchange parameters obtained are summarized in Table 2. It was found that the $\text{Ln}^{\text{III}}-\text{Ln}^{\text{III}}$ exchange interactions for **1**, **2** and **3** are antiferromagnetic. To validate the exchange coupling constants of the $\text{Ln}^{\text{III}}-\text{Ln}^{\text{III}}$ pairs, we have performed DFT calculations for the $\text{Gd}^{\text{III}}-\text{Gd}^{\text{III}}$ pairs (See computational details). The calculations yielded antiferromagnetic exchange

interactions between the Gd^{III} centers, with the *J* value estimated to be -0.04 cm⁻¹, which is in good agreement with the value obtained from Lines model.

The anisotropy barriers were then computed with the lowest energy states of each Ln^{III} ion which were coupled using the POLY_ANISO routine. The energies, the corresponding tunneling gaps and the *g_z* values of the lowest exchange-coupled states of complexes **1** – **3** are given in Tables S5–S6 in the ESI. It is found that the computed barrier energies of each complex correlate nicely with the experimentally determined barriers. For complex **1**, although weak exchange introduces several low lying states, the relaxation is found to occur via excited states lying 78.2 cm⁻¹ above the ground state, due to the tunneling of the magnetization. The coupled state anisotropy barrier; $U_{cal} = 78.2$ cm⁻¹, therefore agrees quite well with the experimentally determined value of 81.2 cm⁻¹ (see Figure 9a).

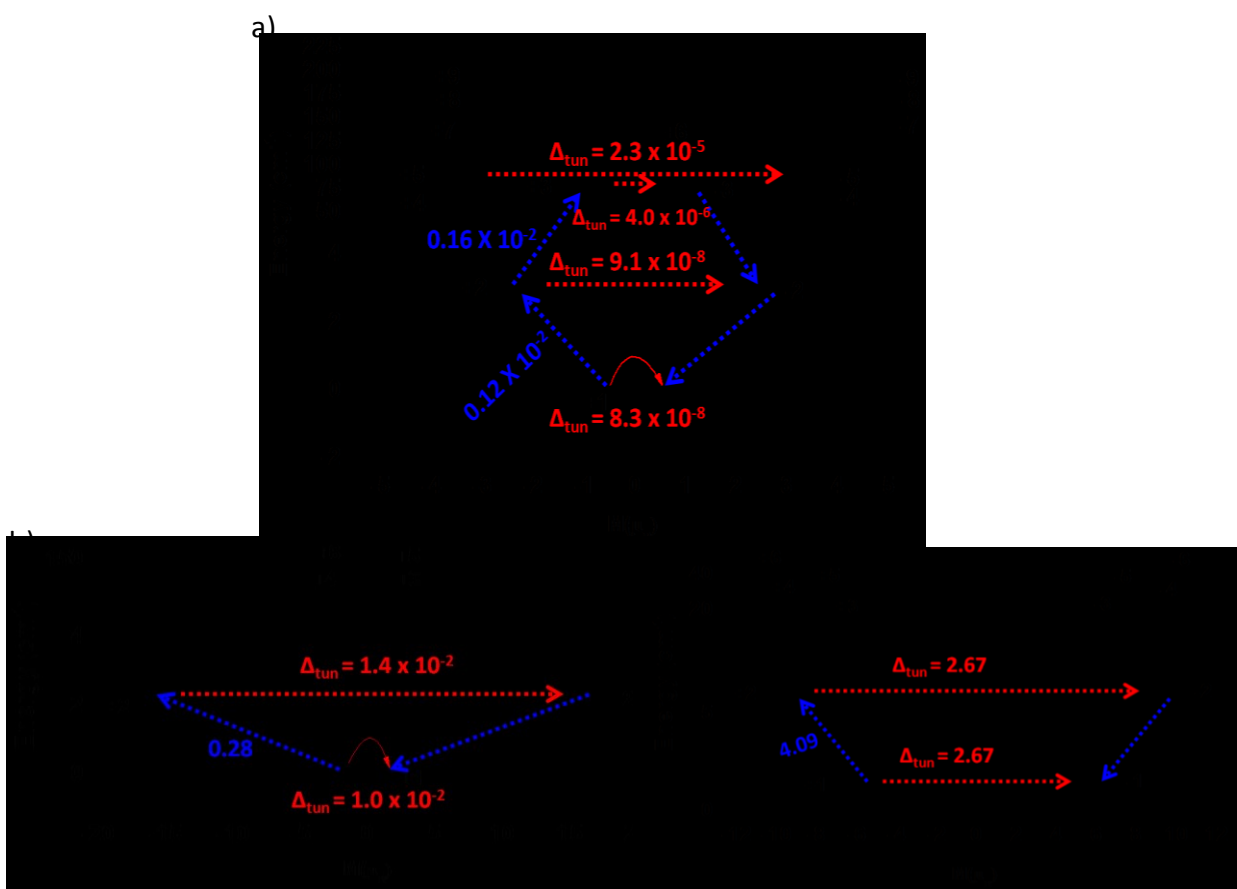


Figure 9. Low-lying exchange spectrum in a) **1**, b) **2** and c) **3**. The exchange states are placed on the diagram according to their magnetic moments (bold black lines). The red arrows show the tunneling transitions (energy splitting) within each doublet state, while the green/blue arrows show the possible pathway through Orbach/Raman relaxation. The numbers at the paths are averaged transition moments in μ_B , connecting the corresponding states.

For complex **2**, on the other hand, the magnetic exchange interaction is not strong enough to quench the quantum tunneling at the ground state, due to the significantly large tunnel splitting still present ($1.0 \times 10^{-2} \text{ cm}^{-1}$, but smaller than the single ion splitting of 0.18 cm^{-1}). This is significantly larger than seen in **1** ($8.3 \times 10^{-8} \text{ cm}^{-1}$). However, the application of a large dc field (5000 Oe) will result in a Zeeman splitting greater than the tunnel splitting leading to quenching of the tunneling, both at the ground and first excited state level, to a certain extent. This will result in relaxation possibly occurring via higher excited states, lying at 138.9 cm^{-1} above the ground state (see Figure 9b). At the third excited state the tunneling splitting ($6.9 \times 10^{-2} \text{ cm}^{-1}$) is very large, therefore the magnetization blockade is unlikely to go higher. The U_{cal} estimate of 138.9 cm^{-1} is, however, much larger than the experimentally determined value of 34.2 cm^{-1} . This discrepancy is due to the fact that complete quenching of the tunneling at the ground and first excited state is unlikely and other non-Orbach mechanisms are also operational in reducing the barrier height.

For complex **3** on the other hand, the ground state tunnel splitting is still exceptionally high (2.67 cm^{-1}), compared to the single ion relaxation mechanism ($2.8 - 4.5 \text{ cm}^{-1}$, see Figure 9c). This is a consequence of the weak $\text{Ho}^{\text{III}}\dots\text{Ho}^{\text{III}}$ magnetic exchange, which displays the smallest J parameter (Table 2) of the three complexes and therefore not strong enough to quench the tunneling of the magnetization. A tunnel splitting of 2.67 cm^{-1} in the ground state suggests that application of a dc field is unlikely to diminish the quantum tunneling relaxation pathway to observe magnetization blockade, concordant with experiments.

Role of diamagnetic substitution in the mechanism of magnetization relaxation:

A large anisotropy barrier (U_{eff}) is found to be present for **1** and its magnitude falls within the range of that previously reported for $\{\text{Co}^{\text{III}}_2\text{Dy}^{\text{III}}_2\}$ SMMs of similar type.¹⁷ We have shown from the

above computational analysis that the electronic structure of the two Dy^{III} single ions reveal the g-tensors in the ground Kramer's doublet are strongly axial with a large g_z value and vanishingly small transverse components (g_x (0.0005), g_y (0.0043)). The SMM behavior is therefore a consequence of this electronic structure. We have therefore, probed how the diamagnetic Co^{III} ion influences the electronic and magnetic behavior and its influence on the U_{eff} value.

To understand the role of the Co^{III} ions, we have created a model where, fictitiously, the Co^{III} ions are removed (complex **1a**, see Figure 5). Calculations reveal that the local g-tensors of the Dy^{III} ions in the ground Kramer's doublet (KDs) are axial in nature, however, now display large transverse components ($g_x = 0.222$, $g_y = 0.521$ and $g_z = 19.419$ for Dy1 and $g_x = 0.370$, $g_y = 1.031$ and $g_z = 19.099$ for Dy2). The computed energies of the first excited Kramer's doublet are found to be 88.5 cm⁻¹ for Dy1, and 71.6 cm⁻¹ for Dy2 (see Table 3). A qualitative mechanism for the magnetic relaxation for the Dy^{III} sites in **1a**, obtained from the *ab initio* calculations is shown in Figures 10a (Dy1) and S4a (Dy2). It can be seen that the tunneling probability in the ground state is now significantly higher for **1a** than for **1** (0.16 vs. 0.8×10^{-3} , respectively, averaged over the two sites). This is essentially due to the presence of large transverse terms in the ground state. To understand the nature of the coupled state, we have assumed the Dy^{III}...Dy^{III} exchange for **1a** to be the same as the complex **1**. The simulated energy levels using the POLY_ANISO routine reveal that the weak Dy^{III}...Dy^{III} exchange is not strong enough to quench the QTM at the ground state and thus **1a** is unlikely to exhibit SMM characteristics. This is supported by various experimental accounts, such as a similar di-hydroxide bridged eight coordinate {Dy^{III}₂} complex which revealed an absence of SMM behaviour.⁴⁴

Table 3. Low-lying energies (cm⁻¹) and g-tensors of Dy^{III} fragments that originate from the corresponding ground atomic multiplet in model complexes **1a – 1d**.

Complex 1a		Complex 1b		Complex 1c		Complex 1d	
Dy1	Dy2	Dy1	Dy1	Dy1	Dy1	Dy1	Dy2
0.0	0.0	0.000	0.000	0.0	0.0	0.000	0.000
88.5	71.6	167.561	168.031	127.2	127.2	47.867	48.499
172.1	132.5	358.937	359.799	288.8	288.8	93.721	94.910
290.8	244.6	455.989	457.620	361.5	361.5	151.855	153.030
445.1	393.0	477.791	479.121	383.3	383.3	171.766	173.200
573.8	529.6	557.047	558.513	465.0	465.0	236.155	237.330
683.7	649.4	612.223	613.395	523.6	523.6	296.710	297.537
1005.2	1007.5	843.870	844.693	780.3	780.3	534.148	534.761

	Ground Kramer's Doublet		Ground Kramer's Doublet		Ground Kramer's Doublet		Ground Kramer's Doublet	
g_x	0.2219	0.3703	0.0002	0.0002	0.0011	0.0011	0.0085	0.0082
g_y	0.5212	1.0312	0.0003	0.0003	0.0015	0.0015	0.0216	0.0210
g_z	19.4198	19.0995	19.9797	19.9124	19.9747	19.9747	19.8339	19.8718

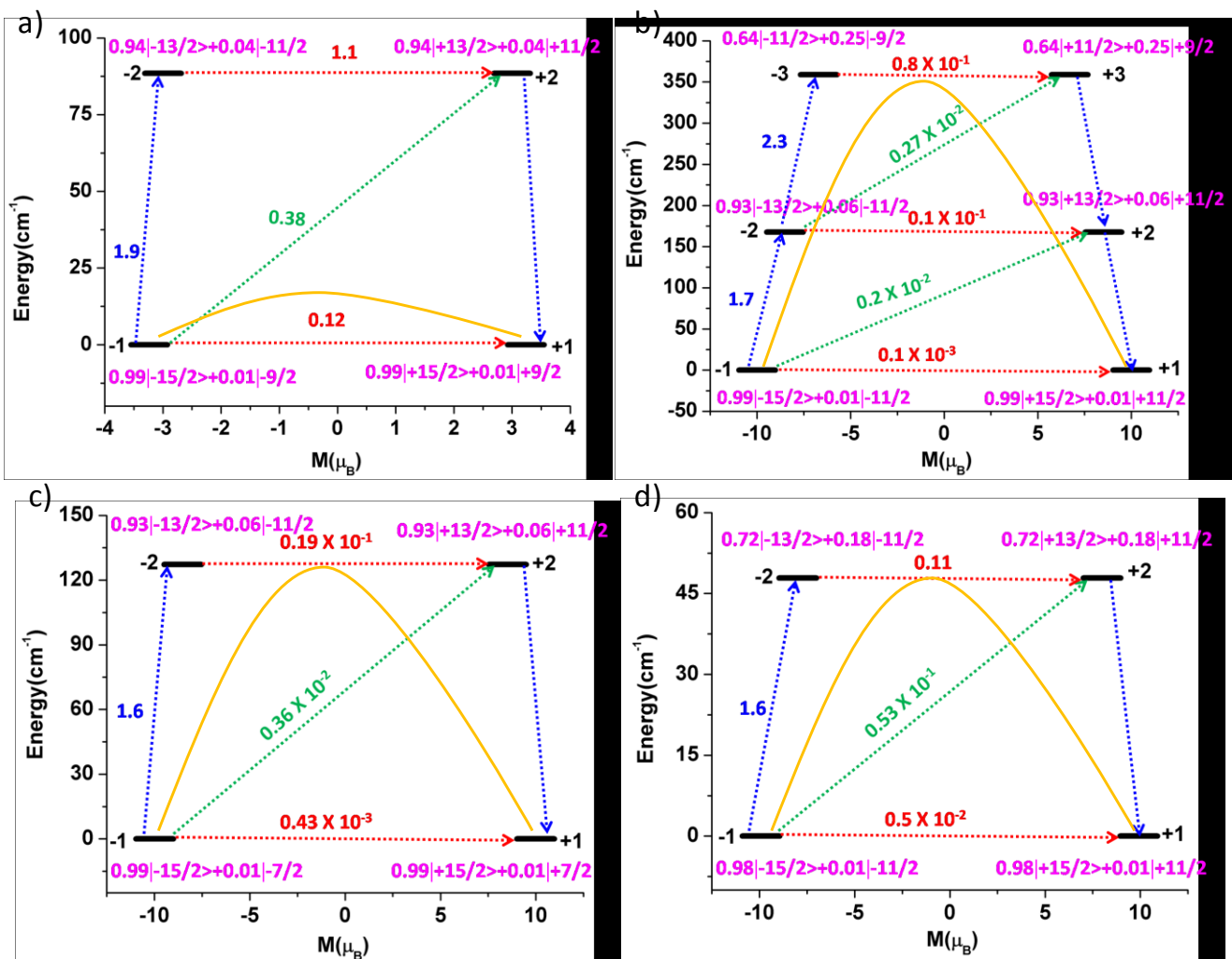


Figure 10. The magnetization blocking barrier for the Dy1 site in a) **1a**; b) **1b**; c) **1c** and d) **1d**. The thick black line indicates the Kramer's doublets (KDs) as a function of computed magnetic moment. The green/blue arrows show the possible pathway through Orbach/Raman relaxation. The dotted red lines represent the presence of QTM/TA-QTM between the connecting pairs. The numbers provided at each arrow are the mean absolute value for the corresponding matrix element of the transition magnetic moment. The yellow curve indicates the most possible relaxation pathway.

While the absence of the trivalent diamagnetic ion suggests the absence of SMM behavior in these complexes, thus highlighting the importance of the diamagnetic ion, we have therefore probed how changing the diamagnetic species might affect the anisotropy barrier and thus SMM properties. We have therefore chosen to replace the tricationic diamagnetic ion in **1**, with monocationic, dicationic and tetracationic diamagnetic ions. We have selected K^I, Zn^{II} and Ti^{IV} as the ions, and modelled the Co^{III} ions in complex **1** as K^I (model **1b**), Zn^{II} (model **1c**) and Ti^{IV} (model **1d**), respectively. The calculations performed for **1b** (see computational details) on both Dy^{III} ions suggest that the local g-tensors in the ground Kramer's doublet (KDs) are pure axial in nature, with very small transverse components ([g_x= 0.0002, g_y= 0.0003 and g_z=19.9797] for Dy1 and [g_x= 0.0002, g_y= 0.0003 and g_z= 19.9124] for Dy2). The presence of a monocationic diamagnetic cation yields very small transverse terms similar to those for **1**, which is contrary to model complex **1a** (no diamagnetic ion) which has a large transverse component. Due to small TA-QTM in the first excited state (tunnel probability $0.1 \times 10^{-1} \mu_B$) the magnetization relaxes via the second excited state (tunnel probability $0.8 \times 10^{-1} \mu_B$) and the computed energies of the Dy^{III} single ion second excited Kramer's doublet for **1b** is found to be 358.9 cm⁻¹ for Dy1, and 359.8 cm⁻¹ for Dy2 (see Table 3). This is larger than that observed for complex **1**, suggesting a stronger electrostatic repulsion offered by the closed-shell K^I ion. A qualitative mechanism for the magnetic relaxation for the Dy^{III} sites in **1b** obtained from the *ab initio* calculations is shown in Figures 10b (Dy1) and S4b (Dy2). If we assume the Dy^{III}...Dy^{III} exchange for **1b** to be of similar magnitude to that in **1**, we can construct an exchange coupled relaxation mechanism (see Figure 11b and Table S8), where a smaller tunneling probability is found in the ground state ($2.4 \times 10^{-10} \text{ cm}^{-1}$), compared to the single-ion analysis of **1b**. Moreover, it is found that the tunneling probability is very small ($9.6 \times$

$10^{-10} - 6.7 \times 10^{-7} \text{ cm}^{-1}$) until the tenth excited state. Therefore, the relaxation pathway proceeds to the eleventh excited state. The effect of the Dy^{III}-Dy^{III} exchange is found to suppress the tunneling for **1b**, compared to the single ion, leading to a barrier height of 361.4 cm⁻¹. This estimate of U_{cal} is larger than that estimated for complex **1** which suggests the superiority of employing a monocationic diamagnetic K^I ion in place of Co^{III}.

Similarly, the calculations performed for **1c** and **1d** (see computational details) on both Dy^{III} ions suggest that the local g-tensors in the ground Kramer's doublet (KDs) are axial in nature, with very small transverse components (See Table 3). Three structurally analogous {Zn^{II}₂Dy^{III}₂} complexes (see ESI Figure S5 for details), possessing eight coordinate Dy^{III} ions have been reported in the literature which offers confidence in our computed model **1c**.⁴⁵ In **1c**, as in the case of complex **1**, the presence of a diamagnetic Zn^{II} cation again yields very small transverse terms. The computed energies of the Dy^{III} single ion first excited Kramer's doublet for **1c** is found to be 127.2 cm⁻¹ for Dy1, and 127.6 cm⁻¹ for Dy2 (see Table 3). This is larger than that observed for complex **1**, but smaller compared to **1b**, suggesting a stronger electrostatic repulsion is also offered by the closed-shell Zn^{II} ion compared to when the Co^{III} ion is present. A qualitative mechanism for the magnetic relaxation for the Dy^{III} sites in **1c** obtained from the *ab initio* calculations is shown in Figures 10c (Dy1) and S4c (Dy2). Clearly, at the single-ion level the QTM effects on the ground state KD (tunnel probability $0.43 \times 10^{-3} \mu_B$) are quenched leading to relaxation via the first excited state, lying at 127 cm⁻¹ above the ground state. For **1c**, we also assumed the Dy^{III}...Dy^{III} exchange for **1c** to be of similar magnitude to that in **1**, and constructed an exchange coupled relaxation mechanism (see Figure 11c and Table S9), where a smaller tunneling probability is found in the ground state ($6.1 \times 10^{-9} \text{ cm}^{-1}$), compared to the single-ion analysis of **1c**. Moreover, it is found that the tunneling probability is also small ($1.8 \times 10^{-8} - 1.1 \times 10^{-7} \text{ cm}^{-1}$) for the first three excited states. Therefore, the relaxation pathway proceeds to the fourth excited state. The effect of the Dy^{III}-Dy^{III} exchange is found to suppress the tunneling for **1c**, compared to the single ion, leading to a barrier height of 129.1 cm⁻¹. These calculations are supported/validated from the experimental observations of the three structurally analogous {Zn^{II}₂Dy^{II}₂} complexes mentioned above, each of which are reported to exhibit SMM characteristics.⁴⁵ In model **1d**, the computed energies of the Dy^{III} single ion first excited Kramer's doublet is found to be 47.9 cm⁻¹ for Dy1, and 48.4 cm⁻¹ for Dy2 (see Table 3, Figures 10d (Dy1) and S4d (Dy2)) which are smaller compared to **1**, **1b** and **1c**. The exchange coupled relaxation mechanism (see Figure 11d and Table S10) suggests that the tunneling

probability is again very small from ground state ($9.5 \times 10^{-7} - 1.9 \times 10^{-5} \text{ cm}^{-1}$) up to the fourth excited state. Thus, the relaxation proceeds via the fourth excited state, leading to a barrier height of 49.6 cm^{-1} . Out of the four diamagnetic ion containing complexes studied the highest charge cation, the Ti^{4+} ion, displays the smallest anisotropy barrier.

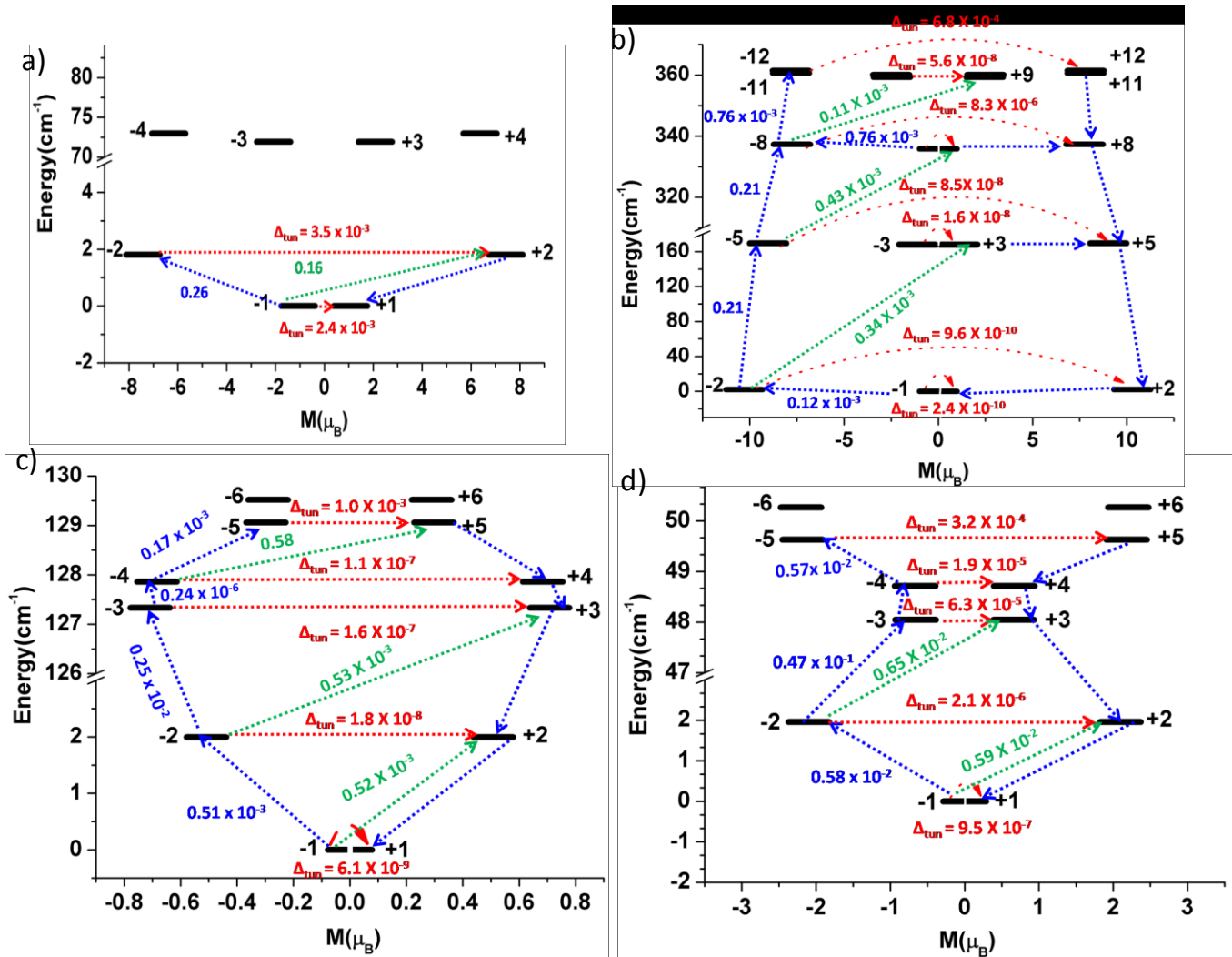


Figure 11. Low-lying exchange spectrum in (a) **1a** (b) **1b** (c) **1c** and (b) **1d**. The exchange states are placed on the diagram according to their magnetic moments (bold black lines). The red arrows show the tunneling transitions (energy splitting) within each doublet state, while the green/blue arrows show the possible pathway through Orbach/Raman relaxation. The numbers at the paths are averaged transition moments in μ_B , connecting the corresponding states.

We have also computed the crystal field (CF) parameters for complexes **1 – 3** and the corresponding models to achieve a deeper insight into the mechanism of magnetic relaxation. The corresponding crystal field Hamiltonian is given in equation 2:

$$\hat{H}_{\text{CF}} = \sum_{k=-q}^q \sum_{k=-q}^q B_k^q \tilde{O}_k^q \dots \quad \text{Eq. 2}$$

Considering that hyperfine interactions and intermolecular interactions are small or negligible, the probability of QTM between the ground state KDs is described by the CF parameters. The corresponding crystal field Hamiltonian is given as Eq. 2, where B_k^q is the crystal field parameter, while O_k^q is the Steven's operator. The QTM effects are dominant in a system where the non-axial B_k^q (in which $q \neq 0$ and $k = 2, 4, 6$) terms are larger than the axial terms (in which $q = 0$ and $k = 2, 4, 6$). The computed CF parameters for complexes **1 – 3** are given in Tables S11 and S13 in the Supporting Information. For all three complexes, **1 – 3**, the non-axial terms are larger than the axial terms reflecting the computed transverse anisotropy for the ground state. The negative sign of the computed B_2^0 parameter reveals the axial character of the ligand field which is determined to be -4.1 (Tb^{III}), -2.4 (Dy^{III}) and -0.56 (Ho^{III}) for **2**, **1** and **3**, respectively. The magnitude of the parameter decreases in the same order as the decrease in oblate character.^{3a, 42} In all cases, significant non-axial terms are detected suggesting prominent QTM effects. If the Co^{III} ions are removed from complex **1** (model **1a**), the non-axial terms are enhanced significantly compared to **1**, leading to a larger transverse anisotropy term and fast QTM relaxation. On the other hand, if a new diamagnetic ion such as K^{I} , Zn^{II} and Ti^{IV} is placed in the position of the Co^{III} ion (model **1b–1d**), the crystal field parameters are very similar to complex **1**, reflecting how the ground state transverse anisotropy are affected by the presence of the diamagnetic ion in the coordination

sphere. A larger barrier, compared to **1**, is calculated in the case of model **1b** and **1c** due to the greater ground-state excited-state gap as the K^I and Zn^{II} ions are found to promote a stronger electrostatic interaction (see Figure 10). This also reflected in the computed Mulliken charges where the K^I and Zn^{II} ions are found to possess a charge of 0.60 and 1.54, while the Co^{III} ion has a charge of 0.75. For the Co^{III} ion the reduction of the computed charge is very large compared to the expected formal value of 3.0, while for K^I and Zn^{II} ions only a moderate deviation from 1.0 and 2.0, respectively is noted. This is likely due to the fact that the empty e_g orbitals of the Co^{III} ion can accept electrons from the coordinating atoms leading to a reduction of the formal charge, while this is not possible for the K^I and Zn^{II} ions. In summary the *ab initio* analysis reveals barrier heights for magnetization reversal are found to be (**1b**, 361.4 cm⁻¹) > (**1c**, 129.1 cm⁻¹) > (**1**, 78.2 cm⁻¹) > (**1d**, 49.6 cm⁻¹) for the diamagnetic ion series. This trend clearly suggests that when the oxidation state of the diamagnetic ion decreases, the electronic repulsion to the bridging atoms increases thus increasing the anisotropy barrier as well as quenching the QTM to a certain extent. The barrier heights are therefore found to correlate to the computed Mulliken charges of the μ₃-OH⁻ bridges which carry a larger negative charge next to the cations of smaller charge (see Figure 8 and Tables S14–S18 and Figures S7–S9 in the Supporting Information). Attempts to isolate compounds similar to that of the model complexes **1b** – **1d** studied here are currently under way in our laboratory.

Conclusions

The synthesis, magnetic and theoretical studies of three tetranuclear {Co^{III}₂Ln^{III}₂} butterfly complexes were carried out. Ac susceptibility measurements revealed the presence of magnetic blocking for **1**, which indicates SMM behavior. An anisotropy barrier U_{eff} of 81.2 cm⁻¹ was determined, with a pure quantum tunneling relaxation time, τ_{QTM} , of ~0.34 s, which suggests that the QTM is fast. The SMM behavior is lost in the absence of a dc field for the Tb^{III} and Ho^{III} analogues, however it can be observed in the presence of a bias direct current field. For Tb^{III} molecule an anisotropy barrier U_{eff} of 34.2 cm⁻¹ was determined under applied field conditions. These experimental observations are rationalized via *ab initio* calculations. The influence of the diamagnetic Co^{III} ion on the relaxation behavior is also probed via *ab initio* and DFT calculations. The evidence strongly suggests that the Co^{III} is integral to the observation of SMM behavior in

these systems and removal of Co^{III} ion found to increase the transverse anisotropy of the ground state leading to a significant QTM relaxation process. Our calculations also predict that other diamagnetic metal ions such as K^I and Zn^{II} in the place of Co^{III}, may yield better performing SMMs, with longer relaxation times as their electrostatic charge polarizations are found to be larger than that computed for Co^{III} ions.

Acknowledgements

KSM thanks the Australian Research Council (ARC) and GR would like to thank DST-SERB (EMR/2014/00024) for funding. Grants to KSM and GR from the Australia-India AISRF fund are gratefully acknowledged. KRV is thankful to the IITB-Monash Research Academy for a PhD studentship. The authors thank Dr. Boujema Moubaraki for help with magnetism. Structural aspects of this research were undertaken on the MX1 beamline at the Australian Synchrotron, Clayton, Victoria, Australia.

References:

1. (a) Christou, G.; Gatteschi, D.; Hendrickson, D. N.; Sessoli, R., Single-molecule magnets. *Mrs Bulletin* **2000**, *25*, 66-71. (b) Sessoli, R.; Gatteschi, D.; Caneschi, A.; Novak, M. A., Magnetic Bistability in a Metal-Ion Cluster. *Nature* **1993**, *365*, 141-143. (c) Sessoli, R.; Tsai, H. L.; Schake, A. R.; Wang, S.; Vincent, J. B.; Folting, K.; Gatteschi, D.; Christou, G.; Hendrickson, D. N., High-spin molecules: [Mn₁₂O₁₂(O₂CR)₁₆(H₂O)₄]. *J. Am. Chem. Soc.* **1993**, *115*, 1804-1816.
2. Sessoli, R.; Powell, A. K., Strategies towards single molecule magnets based on lanthanide ions. *Coord. Chem. Rev.* **2009**, *253*, 2328-2341.
3. (a) Rinehart, J. D.; Long, J. R., Exploiting single-ion anisotropy in the design of f-element single-molecule magnets. *Chem. Sci.* **2011**, *2*, 2078-2085. (b) Sorace, L.; Benelli, C.; Gatteschi, D., Lanthanides in molecular magnetism: old tools in a new field. *Chem. Soc. Rev.* **2011**, *40*, 3092-3104.
4. (a) D. Gatteschi; R. Sessoli; Villain, J., Molecular Nanomagnets. Oxford University Press, Oxford: 2006. (b) Gatteschi, D., Molecular Magnetism: A basis for new materials. *Adv. Mater.* **1994**, *6*, 635-645.
5. (a) Molecular spintronics and quantum computing. *J. Mater. Chem.* **2009**, *19*, 1670-1671. (b) Leuenberger, M. N.; Loss, D., Quantum computing in molecular magnets. *Nature* **2001**, *410*, 789-793.
6. Bogani, L.; Wernsdorfer, W., Molecular spintronics using single-molecule magnets. *Nat. Mater.* **2008**, *7*, 179-186.

7. (a) Blagg, R. J.; Muryn, C. A.; McInnes, E. J. L.; Tuna, F.; Winpenny, R. E. P., Single Pyramid Magnets: Dy₅ Pyramids with Slow Magnetic Relaxation to 40 K. *Angew. Chem. Int. Ed.* **2011**, *123*, 6660-6663. (b) Blagg, R. J.; Tuna, F.; McInnes, E. J. L.; Winpenny, R. E. P., Pentametallic lanthanide-alkoxide square-based pyramids: high energy barrier for thermal relaxation in a holmium single molecule magnet. *Chem. Commun.* **2011**, *47*, 10587-10589. (c) Hewitt, I. J.; Tang, J.; Madhu, N. T.; Anson, C. E.; Lan, Y.; Luzon, J.; Etienne, M.; Sessoli, R.; Powell, A. K., Coupling Dy₃ Triangles Enhances Their Slow Magnetic Relaxation. *Angew. Chem. Int. Ed.* **2010**, *49*, 6352-6356. (d) Lin, P.-H.; Burchell, T. J.; Ungur, L.; Chibotaru, L. F.; Wernsdorfer, W.; Murugesu, M., A Polynuclear Lanthanide Single-Molecule Magnet with a Record Anisotropic Barrier. *Angew. Chem. Int. Ed.* **2009**, *48*, 9489-9492. (e) Liu, J.; Chen, Y.-C.; Liu, J.-L.; Vieru, V.; Ungur, L.; Jia, J.-H.; Chibotaru, L. F.; Lan, Y.; Wernsdorfer, W.; Gao, S.; Chen, X.-M.; Tong, M.-L., A Stable Pentagonal Bipyramidal Dy(III) Single-Ion Magnet with a Record Magnetization Reversal Barrier over 1000 K. *J. Am. Chem. Soc.* **2016**, *138*, 5441-5450.
8. Milios, C. J.; Vinslava, A.; Wernsdorfer, W.; Moggach, S.; Parsons, S.; Perlepes, S. P.; Christou, G.; Brechin, E. K., A Record Anisotropy Barrier for a Single-Molecule Magnet. *J. Am. Chem. Soc.* **2007**, *129*, 2754-2755.
9. (a) Rinehart, J. D.; Fang, M.; Evans, W. J.; Long, J. R., A N₂³⁻ Radical-Bridged Terbium Complex Exhibiting Magnetic Hysteresis at 14 K. *J. Am. Chem. Soc.* **2011**, *133*, 14236-14239. (b) Rinehart, J. D.; Fang, M.; Evans, W. J.; Long, J. R., Strong exchange and magnetic blocking in N₂³⁻ radical-bridged lanthanide complexes. *Nat. Chem.* **2011**, *3*, 538-542.
10. Gupta, S. K.; Rajeshkumar, T.; Rajaraman, G.; Murugavel, R., An air-stable Dy(III) single-ion magnet with high anisotropy barrier and blocking temperature. *Chem. Sci.* **2016**, *7*, 5181-5191.
11. (a) Langley, S. K.; Moubaraki, B.; Murray, K. S., A heptadecanuclear Mn^{III}₉Dy^{III}₈ cluster derived from triethanolamine with two edge sharing supertetrahedra as the core and displaying SMM behaviour. *Dalton Trans.* **2010**, *39*, 5066-5069. (b) Rigaux, G.; Inglis, R.; Morrison, S.; Prescimone, A.; Cadiou, C.; Evangelisti, M.; Brechin, E. K., Enhancing Ueff in oxime-bridged [Mn^{III}₆Ln^{III}₂] hexagonal prisms. *Dalton Trans.* **2011**, *40*, 4797-4799.
12. (a) Langley, S. K.; Wielechowski, D. P.; Moubaraki, B.; Murray, K. S., Enhancing the magnetic blocking temperature and magnetic coercivity of {Cr^{III}₂Ln^{III}₂} single-molecule magnets via bridging ligand modification. *Chem. Commun.* **2016**, *52*, 10976-10979. (b) Langley, S. K.; Wielechowski, D. P.; Vieru, V.; Chilton, N. F.; Moubaraki, B.; Abrahams, B. F.; Chibotaru, L. F.; Murray, K. S., A {Cr^{III}₂Dy^{III}₂} Single-Molecule Magnet: Enhancing the Blocking Temperature through 3d Magnetic Exchange. *Angew. Chem. Int. Ed.* **2013**, *52*, 12014-12019.
13. Schray, D.; Abbas, G.; Lan, Y.; Mereacre, V.; Sundt, A.; Dreiser, J.; Waldmann, O.; Kostakis, G. E.; Anson, C. E.; Powell, A. K., Magnetische Suszeptibilitätsmessung und ⁵⁷Fe-Mößbauer-Spektroskopie an einem ferromagnetischen Fe^{III}₄Dy₄-Ring. *Angew. Chem. Int. Ed.* **2010**, *122*, 5312-5315.
14. (a) Li, M.; Ako, A. M.; Lan, Y.; Wernsdorfer, W.; Buth, G.; Anson, C. E.; Powell, A. K.; Wang, Z.; Gao, S., New heterometallic [Mn^{III}₄Ln^{III}₄] wheels incorporating formate ligands. *Dalton Trans.* **2010**, *39*, 3375-3377. (b) Li, M.; Lan, Y.; Ako, A. M.; Wernsdorfer, W.; Anson, C. E.; Buth, G.; Powell, A. K.; Wang, Z.; Gao, S., A Family of 3d-4f Octa-Nuclear [Mn^{III}₄Ln^{III}₄] Wheels (Ln = Sm, Gd, Tb, Dy, Ho, Er, and Y): Synthesis, Structure, and Magnetism. *Inorg. Chem.* **2010**, *49*, 11587-11594. (c) Vignesh, K. R.; Langley, S. K.; Moubaraki, B.; Murray, K. S.; Rajaraman, G., Large Hexadecametallic {Mn^{III}-Ln^{III}} Wheels: Synthesis, Structural, Magnetic, and Theoretical Characterization. *Chem. Eur. J.* **2015**, *21*, 16364-16369.

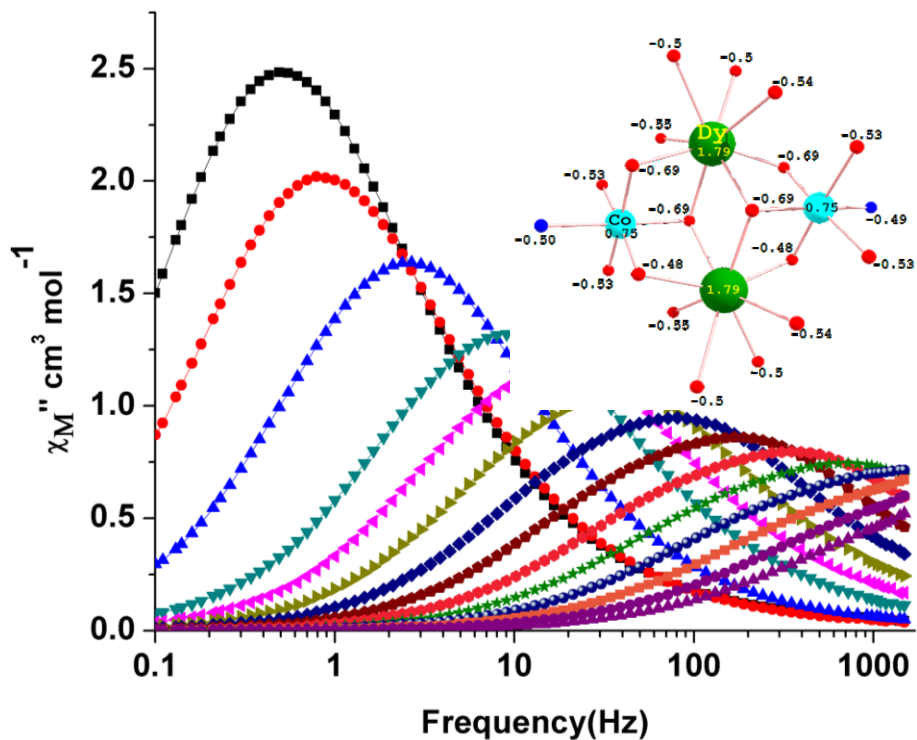
15. (a) Ahmed, N.; Das, C.; Vaidya, S.; Langley, S. K.; Murray, K. S.; Shanmugam, M., Nickel(II)-Lanthanide(III) Magnetic Exchange Coupling Influencing Single-Molecule Magnetic Features in $\{Ni_2Ln_2\}$ Complexes. *Chem. Eur. J.* **2014**, *20*, 14235-14239. (b) Chandrasekhar, V.; Bag, P.; Kroener, W.; Gieb, K.; Müller, P., Pentanuclear Heterometallic $\{Ni_2Ln_3\}$ ($Ln = Gd, Dy, Tb, Ho$) Assemblies. Single-Molecule Magnet Behavior and Multistep Relaxation in the Dysprosium Derivative. *Inorg. Chem.* **2013**, *52*, 13078-13086.
16. (a) Oyarzabal, I.; Ruiz, J.; Ruiz, E.; Aravena, D.; Seco, J. M.; Colacio, E., Increasing the effective energy barrier promoted by the change of a counteranion in a Zn-Dy-Zn SMM: slow relaxation via the second excited state. *Chem. Commun.* **2015**, *51*, 12353-12356. (b) Costes, J. P.; Titos-Padilla, S.; Oyarzabal, I.; Gupta, T.; Duhayon, C.; Rajaraman, G.; Colacio, E., Analysis of the Role of Peripheral Ligands Coordinated to Zn^{II} in Enhancing the Energy Barrier in Luminescent Linear Trinuclear Zn-Dy-Zn Single-Molecule Magnets. *Chem. Eur. J.* **2015**, *21*, 15785-15796. (c) Costes, J. P.; Titos-Padilla, S.; Oyarzabal, I.; Gupta, T.; Duhayon, C.; Rajaraman, G.; Colacio, E., Effect of Ligand Substitution around the Dy^{III} on the SMM Properties of Dual-Luminescent Zn-Dy and Zn-Dy-Zn Complexes with Large Anisotropy Energy Barriers: A Combined Theoretical and Experimental Magnetostructural Study. *Inorg. Chem.* **2016**, *55*, 4428-4440. (d) Upadhyay, A.; Singh, S. K.; Das, C.; Mondol, R.; Langley, S. K.; Murray, K. S.; Rajaraman, G.; Shanmugam, M., Enhancing the effective energy barrier of a Dy(iii) SMM using a bridged diamagnetic Zn(ii) ion. *Chem. Commun.* **2014**, *50*, 8838-8841.
17. (a) Langley, S. K.; Chilton, N. F.; Moubaraki, B.; Murray, K. S., Anisotropy barrier enhancement via ligand substitution in tetranuclear $\{Co^{III}_2Ln^{III}_2\}$ single molecule magnets. *Chem. Commun.* **2013**, *49*, 6965-6967. (b) Langley, S. K.; Chilton, N. F.; Moubaraki, B.; Murray, K. S., Single-Molecule Magnetism in Three Related $\{Co^{III}_2Dy^{III}_2\}$ -Acetylacetone Complexes with Multiple Relaxation Mechanisms. *Inorg. Chem.* **2013**, *52*, 7183-7192. (c) Langley, S. K.; Chilton, N. F.; Moubaraki, B.; Murray, K. S., Single-molecule magnetism in $\{Co^{III}_2Dy^{III}_2\}$ -amine-polyalcohol-acetylacetone complexes: effects of ligand replacement at the Dy^{III} sites on the dynamics of magnetic relaxation. *Inorg. Chem. Front.* **2015**, *2*, 867-875. (d) Langley, S. K.; Chilton, N. F.; Ungur, L.; Moubaraki, B.; Chibotaru, L. F.; Murray, K. S., Heterometallic Tetranuclear $[Ln^{III}_2Co^{III}_2]$ Complexes Including Suppression of Quantum Tunneling of Magnetization in the $[Dy^{III}_2Co^{III}_2]$ Single Molecule Magnet. *Inorg. Chem.* **2012**, *51*, 11873-11881. (e) Langley, S. K.; Ungur, L.; Chilton, N. F.; Moubaraki, B.; Chibotaru, L. F.; Murray, K. S., Single-Molecule Magnetism in a Family of $\{Co^{III}_2Dy^{III}_2\}$ Butterfly Complexes: Effects of Ligand Replacement on the Dynamics of Magnetic Relaxation. *Inorg. Chem.* **2014**, *53*, 4303-4315.
18. Cowieson, N. P.; Aragao, D.; Clift, M.; Ericsson, D. J.; Gee, C.; Harrop, S. J.; Mudie, N.; Panjikar, S.; Price, J. R.; Riboldi-Tunnicliffe, A.; Williamson, R.; Caradoc-Davies, T., MX1: a bending-magnet crystallography beamline serving both chemical and macromolecular crystallography communities at the Australian Synchrotron. *J. Synchrotron Radiat.* **2015**, *22*, 187-190.
19. McPhillips, T. M.; McPhillips, S. E.; Chiu, H.-J.; Cohen, A. E.; Deacon, A. M.; Ellis, P. J.; Garman, E.; Gonzalez, A.; Sauter, N. K.; Phizackerley, R. P.; Soltis, S. M.; Kuhn, P., Blu-Ice and the Distributed Control System: software for data acquisition and instrument control at macromolecular crystallography beamlines. *J. Synchrotron Radiat.* **2002**, *9*, 401-406.
20. Kabsch, W., Automatic processing of rotation diffraction data from crystals of initially unknown symmetry and cell constants. *J. Appl. Crystallogr.* **1993**, *26*, 795-800.
21. Sheldrick, G., A short history of SHELX. *Acta Crystallogr. Sect. A* **2008**, *64*, 112-122.

22. Sheldrick, G. M., *SHELXL-97, Programs for X-ray Crystal Structure Refinement*; **1997**, University of Göttingen: Göttingen, Germany, .
23. Barbour, L. J., *J. Supramol. Chem.* **2001**, *1*, 189-191.
24. Aquilante, F.; Pedersen, T. B.; Veryazov, V.; Lindh, R., MOLCAS—a software for multiconfigurational quantum chemistry calculations. *WIREs Comput. Mol. Sci.* **2013**, *3*, 143-149.
25. Hess, B. A.; Marian, C. M.; Wahlgren, U.; Gropen, O., A mean-field spin-orbit method applicable to correlated wavefunctions. *Chem. Phys. Lett.* **1996**, *251*, 365-371.
26. Roos, B. O.; Malmqvist, P.-A., Relativistic quantum chemistry: the multiconfigurational approach. *Phys. Chem. Chem. Phys.* **2004**, *6*, 2919-2927.
27. Roos, B. O.; Lindh, R.; Malmqvist, P.-A.; Veryazov, V.; Widmark, P.-O.; Borin, A. C., New Relativistic Atomic Natural Orbital Basis Sets for Lanthanide Atoms with Applications to the Ce Diatom and LuF₃. *J. Phys. Chem. A* **2008**, *112*, 11431-11435.
28. Malmqvist, P. A.; Roos, B. O.; Schimmelpfennig, B., The restricted active space (RAS) state interaction approach with spin-orbit coupling. *Chem. Phys. Lett.* **2002**, *357*, 230-240.
29. Chibotaru, L. F.; Ungur, L., Ab initio calculation of anisotropic magnetic properties of complexes. I. Unique definition of pseudospin Hamiltonians and their derivation. *J. Chem. Phys.* **2012**, *137*, 064112-22.
30. Chibotaru, L. F.; Ungur, L., *Program POLY_ANISO 2006*, University of Leuven.
31. Noddeman, L., Valence bond description of antiferromagnetic coupling in transition metal dimers. *J. Am. Chem. Soc.* **1981**, *74*, 5737-5743.
32. (a) Christian, P.; Rajaraman, G.; Harrison, A.; Helliwell, M.; McDouall, J. J. W.; Raftery, J.; Winpenny, R. E. P., Synthesis and studies of a trinuclear Mn(ii) carboxylate complex. *Dalton Trans.* **2004**, 2550-2555. (b) Piligkos, S.; Rajaraman, G.; Soler, M.; Kirchner, N.; van Slageren, J.; Bircher, R.; Parsons, S.; Gudel, H.-U.; Kortus, J.; Wernsdorfer, W.; Christou, G.; Brechin, E. K., Studies of an Enneanuclear Manganese Single-Molecule Magnet. *J. Am. Chem. Soc.* **2005**, *127*, 5572-5580. (c) Rajaraman, G.; Cano, J.; Brechin, E. K.; McInnes, E. J. L., Density functional calculations of a tetradecametallic iron(iii) cluster with a very large spin ground state. *Chem. Commun.* **2004**, 1476-1477. (d) Ruiz, E.; Cano, J.; Alvarez, S.; Alemany, P., Broken symmetry approach to calculation of exchange coupling constants for homobinuclear and heterobinuclear transition metal complexes. *J. Comput. Chem.* **1999**, *20*, 1391-1400. (e) Ruiz, E.; Cano, J.; Alvarez, S.; Caneschi, A.; Gatteschi, D., Theoretical Study of the Magnetic Behavior of Hexanuclear Cu(II) and Ni(II) Polysiloxanolate Complexes. *J. Am. Chem. Soc.* **2003**, *125*, 6791-6794. (f) Ruiz, E.; Rodríguez-Forteá, A.; Cano, J.; Alvarez, S.; Alemany, P., About the calculation of exchange coupling constants in polynuclear transition metal complexes. *J. Comput. Chem.* **2003**, *24*, 982-989.
33. (a) Berg, N.; Hooper, T. N.; Liu, J.; Beedle, C. C.; Singh, S. K.; Rajaraman, G.; Piligkos, S.; Hill, S.; Brechin, E. K.; Jones, L. F., Synthetic, structural, spectroscopic and theoretical study of a Mn(iii)-Cu(ii) dimer containing a Jahn-Teller compressed Mn ion. *Dalton Trans.* **2013**, *42*, 207-216. (b) Berg, N.; Rajeshkumar, T.; Taylor, S. M.; Brechin, E. K.; Rajaraman, G.; Jones, L. F., What Controls the Magnetic Interaction in bis- μ -Alkoxo Mn^{III} Dimers? A Combined Experimental and Theoretical Exploration. *Chem. Eur. J.* **2012**, *18*, 5906-5918. (c) Ghosh, S.; Singh, S. K.; Tewary, S.; Rajaraman, G., Enhancing the double exchange interaction in a mixed valence {V^{III}-V^{II}} pair: a theoretical perspective. *Dalton Trans.* **2013**, *42*, 16490-16493. (d) Rajaraman, G.; Murugesu, M.; Sanudo, E. C.; Soler, M.; Wernsdorfer, W.; Helliwell, M.; Muryn, C.; Raftery, J.; Teat, S. J.; Christou, G.; Brechin, E. K., A Family of Manganese Rods: Syntheses, Structures, and Magnetic Properties. *J. Am. Chem. Soc.* **2004**, *126*, 15445-15457.

34. (a) Baker, M. L.; Timco, G. A.; Piligkos, S.; Mathieson, J. S.; Mutka, H.; Tuna, F.; Kozlowski, P.; Antkowiak, M.; Guidi, T.; Gupta, T.; Rath, H.; Woolfson, R. J.; Kamieniarz, G.; Pritchard, R. G.; Weihe, H.; Cronin, L.; Rajaraman, G.; Collison, D.; McInnes, E. J. L.; Winpenny, R. E. P., A classification of spin frustration in molecular magnets from a physical study of large odd-numbered-metal, odd electron rings. *Proc. Natl. Acad. Sci. USA* **2012**, *109*, 19113-19118. (b) Christian, P.; Rajaraman, G.; Harrison, A.; McDouall, J. J. W.; Raftery, J. T.; Winpenny, R. E. P., Structural, magnetic and DFT studies of a hydroxide-bridged {Cr₈} wheel. *Dalton Trans.* **2004**, 1511-1512. (c) Cremades, E.; Cano, J.; Ruiz, E.; Rajaraman, G.; Milios, C. J.; Brechin, E. K., Theoretical Methods Enlighten Magnetic Properties of a Family of Mn₆ Single-Molecule Magnets. *Inorg. Chem.* **2009**, *48*, 8012-8019. (d) Vignesh, K. R.; Langley, S. K.; Murray, K. S.; Rajaraman, G., What Controls the Magnetic Exchange Interaction in Mixed- and Homo-Valent Mn₇ Disc-Like Clusters? A Theoretical Perspective. *Chem. Eur. J.* **2015**, *21*, 2881-2892.
35. Becke, A. D., Density functional thermochemistry. III. The role of exact exchange. *J. Chem. Phys.* **1993**, *98*, 5648-5652.
36. **Gaussian 09, R. A.02**, Frisch, M. J. ; G. W. Trucks; H. B. Schlegel; G. E. Scuseria; M. A. Robb; J. R. Cheeseman; G. Scalmani; V. Barone; B. Mennucci; G. A. Petersson; H. Nakatsuji; M. Caricato; X. Li; H. P. Hratchian; A. F. Izmaylov; J. Bloino; G. Zheng; J. L. Sonnenberg; M. Hada; M. Ehara; K. Toyota; R. Fukuda; J. Hasegawa; M. Ishida; T. Nakajima; Y. Honda; O. Kitao; H. Nakai; T. Vreven; J. A. Montgomery; Jr., J. E. P.; F. Ogliaro; M. Bearpark; J. J. Heyd; E. Brothers; K. N. Kudin; V. N. Staroverov; R. Kobayashi; J. Normand; K. Raghavachari; A. Rendell; J. C. Burant; S. S. Iyengar; J. Tomasi; M. Cossi; N. Rega; J. M. Millam; M. Klene; J. E. Knox; J. B. Cross; V. Bakken; C. Adamo; J. Jaramillo; R. Gomperts; R. E. Stratmann; O. Yazyev; A. J. Austin; R. Cammi; C. Pomelli; J. W. Ochterski; R. L. Martin; K. Morokuma; V. G. Zakrzewski; G. A. Voth; P. Salvador; J. J. Dannenberg; S. Dapprich; A. D. Daniels; Ö. Farkas; J. B. Foresman; J. V. Ortiz; J. Cioslowski, a.; D. J. Fox; Gaussian, I., Wallingford CT . **2009**.
37. Cundari, T. R.; Stevens, W. J., Effective core potential methods for the lanthanides. *J. Chem. Phys.* **1993**, *98*, 5555-5565.
38. (a) Schaefer, A.; Horn, H.; Ahlrichs, R., Fully optimized contracted Gaussian basis sets for atoms Li to Kr. *J. Chem. Phys.* **1992**, *97*, 2571-2577. (b) Schaefer, A.; Huber, C.; Ahlrichs, R., Fully optimized contracted Gaussian basis sets of triple zeta valence quality for atoms Li to Kr. *J. Chem. Phys.* **1994**, *100*, 5829-5835.
39. Langley, S. K.; Le, C.; Ungur, L.; Moubaraki, B.; Abrahams, B. F.; Chibotaru, L. F.; Murray, K. S., Heterometallic 3d–4f Single-Molecule Magnets: Ligand and Metal Ion Influences on the Magnetic Relaxation. *Inorg. Chem.* **2015**, *54*, 3631-3642.
40. (a) Cirera, J.; Ruiz, E.; Alvarez, S., Shape and Spin State in Four-Coordinate Transition-Metal Complexes: The Case of the d₆ Configuration. *Chem. Eur. J.* **2006**, *12*, 3162-3167. (b) Pinsky, M.; Avnir, D., Continuous Symmetry Measures. 5. The Classical Polyhedra. *Inorg. Chem.* **1998**, *37*, 5575-5582.
41. (a) Feltham, H. L. C.; Klower, F.; Cameron, S. A.; Larsen, D. S.; Lan, Y.; Tropiano, M.; Faulkner, S.; Powell, A. K.; Brooker, S., A family of 13 tetranuclear zinc(ii)-lanthanide(iii) complexes of a [3 + 3] Schiff-base macrocycle derived from 1,4-diformyl-2,3-dihydroxybenzene. *Dalton Trans.* **2011**, *40*, 11425-11432. (b) Yamashita, A.; Watanabe, A.; Akine, S.; Nabeshima, T.; Nakano, M.; Yamamura, T.; Kajiwara, T., Wheel-Shaped Er^{III}Zn^{II3} Single-Molecule Magnet: A Macroyclic Approach to Designing Magnetic Anisotropy. *Angew. Chem. Int. Ed.* **2011**, *50*, 4016-4019.

42. Gupta, T.; Velmurugan, G.; Rajeshkumar, T.; Rajaraman, G., Role of Lanthanide-Ligand bonding in the magnetization relaxation of mononuclear single-ion magnets: A case study on Pyrazole and Carbene ligated Ln^{III} (Ln=Tb, Dy, Ho, Er) complexes. *J. Chem. Sci.* **2016**, *128*, 1615-1630.
43. Lines, M. E., Orbital Angular Momentum in the Theory of Paramagnetic Clusters. *J. Chem. Phys.* **1971**, *55*, 2977-2984.
44. Zhou, Q.; Yang, F.; Liu, D.; Peng, Y.; Li, G.; Shi, Z.; Feng, S., Synthesis, Structures, and Magnetic Properties of Three Fluoride-Bridged Lanthanide Compounds: Effect of Bridging Fluoride Ions on Magnetic Behaviors. *Inorg. Chem.* **2012**, *51*, 7529-7536.
45. (a) Yu, W.-R.; Lee, G.-H.; Yang, E.-C., Systematic studies of the structures and magnetic properties for a family of cubane complexes with the formula: [M₂Ln₂] (Ln = Dy, Gd; M = Ni, Zn) and [Ni₂Y₂]. *Dalton Trans.* **2013**, *42*, 3941-3949. (b) Abtab, S. M. T.; Maity, M.; Bhattacharya, K.; Sañudo, E. C.; Chaudhury, M., Syntheses, Structures, and Magnetic Properties of a Family of Tetranuclear Hydroxido-Bridged Ni^{II}₂Ln^{III}₂ (Ln = La, Gd, Tb, and Dy) Complexes: Display of Slow Magnetic Relaxation by the Zinc(II)-Dysprosium(III) Analogue. *Inorg. Chem.* **2012**, *51*, 10211-10221. (c) Meng, Z.-S.; Guo, F.-S.; Liu, J.-L.; Leng, J.-D.; Tong, M.-L., Heterometallic cubane-like {M₂Ln₂} (M = Ni, Zn; Ln = Gd, Dy) and {Ni₂Y₂} aggregates. Synthesis, structures and magnetic properties. *Dalton Trans.* **2012**, *41*, 2320-2329.

Table of contents



A combined experimental and theoretical study on a series of $\{\text{Co}^{\text{III}}_2\text{Ln}^{\text{III}}_2\}$ ($\text{Ln} = \text{Dy}, \text{Tb}$ and Ho) complexes “butterfly” complexes unveils ways to enhance the SMM behavior in $\{3\text{d}-4\text{f}\}$ complexes by utilizing the 3d diamagnetic ions.